The Plant Cell, Vol. 25: 3405–3423, September 2013, www.plantcell.org

Arabidopsis ACTIN-DEPOLYMERIZING FACTOR7 Severs Actin Filaments and Regulates Actin Cable Turnover to Promote Normal Pollen Tube Growth[W]

Yiyan Zheng,[a,b,1] Yurong Xie,[a,1] Yuxiang Jiang,[a,b,1] Xiaolu Qu,[a,b] and Shanjin Huang[a,c,2]

[a] Key Laboratory of Plant Molecular Physiology, Institute of Botany, Chinese Academy of Sciences, Beijing 100093, China
[b] University of Chinese Academy of Sciences, Beijing 100049, China
[c] National Center for Plant Gene Research, Beijing 100101, China

ORCID ID: 0000-0001-9517-2515 (S.H.).

Actin filaments are often arranged into higher-order structures, such as the longitudinal actin cables that generate the reverse fountain cytoplasmic streaming pattern present in pollen tubes. While several actin binding proteins have been implicated in the generation of these cables, the mechanisms that regulate their dynamic turnover remain largely unknown. Here, we show that *Arabidopsis thaliana* ACTIN-DEPOLYMERIZING FACTOR7 (ADF7) is required for turnover of longitudinal actin cables. In vitro biochemical analyses revealed that ADF7 is a typical ADF that prefers ADP-G-actin over ATP-G-actin. ADF7 inhibits nucleotide exchange on actin and severs filaments, but its filament severing and depolymerizing activities are less potent than those of the vegetative ADF1. ADF7 primarily decorates longitudinal actin cables in the shanks of pollen tubes. Consistent with this localization pattern, the severing frequency and depolymerization rate of filaments significantly decreased, while their maximum lifetime significantly increased, in *adf7* pollen tube shanks. Furthermore, an ADF7–enhanced green fluorescent protein fusion with defective severing activity but normal G-actin binding activity could not complement *adf7*, providing compelling evidence that the severing activity of ADF7 is vital for its in vivo functions. These observations suggest that ADF7 evolved to promote turnover of longitudinal actin cables by severing actin filaments in pollen tubes.

INTRODUCTION

The actin cytoskeleton constantly undergoes dynamic assembly and disassembly. These dynamic changes allow cells to constantly remodel networks and build distinct structures needed for various physiological cellular processes, including cell motility, cell division, cytokinesis, maintenance of cell polarity, and polarized cell growth (Pollard and Cooper, 2009), as well as responses to various stimuli (Staiger, 2000). How diverse cellular actin structures are generated and remodeled remains an open question in cell biology.

The pollen tube extends rapidly through the style, searching for the ovule in order to deliver two nonmotile sperm cells, resulting in double fertilization in flowering plants. Growth of the pollen tube is highly dependent upon dynamic remodeling of the actin cytoskeleton (Taylor and Hepler, 1997; Gibbon et al., 1999; Hepler et al., 2001; Vidali and Hepler, 2001; Vidali et al., 2001). It is widely accepted that the actin cytoskeleton is arranged into at least three distinct structures within pollen tubes (Cheung and Wu, 2008; Chen et al., 2009; Staiger et al., 2010). In the shank region, longitudinal actin cables are distributed throughout the cytoplasm. The consensus view regarding the function of longitudinal actin cables is that they provide molecular tracks to drive intracellular trafficking events, such as organelle movement and vesicle trafficking.

Several actin binding proteins have been implicated in the generation of longitudinal actin cables in the pollen tube. For example, the formin protein *Arabidopsis thaliana* Formin3 nucleates actin assembly (Ye et al., 2009), while bundling proteins, such as fimbrins, villins, and LIM-domain–containing proteins, decorate and stabilize actin cables, as well as maintaining their longitudinal arrangement (Wang et al., 2008; Papuga et al., 2010; Wu et al., 2010; Zhang et al., 2010; Su et al., 2012; Qu et al., 2013). However, the mechanisms that facilitate dynamic remodeling of these longitudinal actin cables and the extent to which dynamics of longitudinal actin cables are related to pollen tube growth remain largely unknown.

ACTIN-DEPOLYMERIZING FACTOR (ADF)/cofilin is a major factor involved in actin depolymerization and serves as a limiting factor in rapid actin turnover. ADF was originally purified from embryonic chicken brain (Bamburg et al., 1980) and was subsequently shown to rapidly depolymerize filamentous actin (Giuliano et al., 1988). Homologs of ADF have been identified in many different species, including plants. Although one ADF and one ADF and two cofilins are encoded in the genomes of unicellular eukaryotes and vertebrates, respectively, the number of *ADF* genes is significantly expanded in flowering plants (Maciver and Hussey, 2002; Feng et al., 2006; Bamburg and Bernstein, 2008). There are a total of 11 *ADF* genes encoded by the *Arabidopsis* genome, and these genes can be divided into four subclasses (Ruzicka et al., 2007). *Arabidopsis ADF*s have been implicated in numerous physiological processes, including etiolated

[1] These authors contributed equally to this work.
[2] Address correspondence to sjhuang@ibcas.ac.cn.
The author responsible for distribution of materials integral to the findings presented in this article in accordance with the policy described in the Instructions for Authors (www.plantcell.org) is: Shanjin Huang (sjhuang@ibcas.ac.cn).
[W] Online version contains Web-only data.
www.plantcell.org/cgi/doi/10.1105/tpc.113.117820

hypocotyl growth, seedling development, flower timing, root hair growth, and plant defense (Dong et al., 2001; Gilliland et al., 2003; Burgos-Rivera et al., 2008; Clément et al., 2009; Tian et al., 2009; Henty et al., 2011). ADF has also been implicated in polarized moss protonemal cell growth (Augustine et al., 2008) and pollen tube growth (Chen et al., 2002; Li et al., 2010). However, knowledge regarding potential functions of ADF in pollen tube growth has primarily been obtained from gain-of-function studies (Chen et al., 2002; Li et al., 2010). Due to the presence of several distinct actin arrays and coexistence of multiple ADF isovariants (Bou Daher et al., 2011; Daher and Geitmann, 2012), loss-of-function analysis is needed to better understand the precise functions and mechanisms of action of each ADF isovariant during pollen tube growth. *Arabidopsis ADF7* and *ADF10* belong to the class IIa *ADFs*, which are expressed specifically in pollen (Pina et al., 2005; Ruzicka et al., 2007). Green fluorescent protein (GFP) fusions of both ADF7 and ADF10 were shown to decorate actin filaments and exhibit distinct localization patterns within pollen tubes (Bou Daher et al., 2011; Daher and Geitmann, 2012). However, whether these GFP fusion proteins are fully functional in the pollen tube needs to be examined. Furthermore, their precise roles in regulation of actin dynamics during pollen tube growth remain to be determined.

The biochemical activities of ADF/cofilins have been documented extensively over the past several decades. ADF/cofilin is able to bind to both ADP- and ATP-loaded G-actin, but it prefers ADP-loaded G-actin and inhibits nucleotide exchange (Carlier et al., 1997; Tian et al., 2009). Therefore, ADF/cofilin was thought to target older actin filaments. Historically, ADF/cofilin was thought to be an actin-depolymerizing protein that promoted subunit dissociation from the pointed ends of actin filaments (Carlier et al., 1997). However, more recent evidence suggests that filament severing is the primary mechanism required for the function of ADF/cofilins (Andrianantoandro and Pollard, 2006; Chen and Pollard, 2011; Henty et al., 2011; Suarez et al., 2011). The most compelling evidence comes from the results showing that specific abolishment of the severing activity of cofilin through point mutations alters its function in vivo (Chen and Pollard, 2011). However, to date, no similar study has been reported in plants. Previous studies have shown that the biochemical activities of ADF isovariants can vary greatly (Tholl et al., 2011), emphasizing the importance of characterizing the biochemical activity of each isovariant carefully before assessing its function in vivo. For example, a previous study showed that lily (*Lilium longiflorum*) pollen ADF1 binds to F-actin better and has less depolymerizing activity than the vegetative maize (*Zea mays*) ADF3 (Smertenko et al., 2001). However, more evidence is needed to determine whether these differences in activity are a common phenomenon for pollen ADFs. In particular, careful comparison of pollen and vegetative ADF isovariants from the same species is an ideal means to test this notion. Furthermore, careful determination of the interactions of pollen ADF with G-actin and F-actin and comparison of any differences in activity between pollen and vegetative ADF in regulation of the turnover of single actin filaments are necessary to better understand the mechanism of action of pollen ADF within the pollen cellular context.

To characterize the molecular mechanisms underlying the dynamic turnover of longitudinal actin cables in pollen tubes, we analyzed the role of pollen-specific ADF7 in *Arabidopsis* using a combination of live-cell imaging, reverse genetics, and state-of-the-art biochemical assays. Our results demonstrate that ADF7 is a typical ADF, but that it is less potent than the vegetative ADF1, consistent with several previous reports (Lopez et al., 1996; Smertenko et al., 2001; Allwood et al., 2002). These observations suggest that weak depolymerizing activity may be commonly associated with pollen ADFs, implying that these proteins may have evolved to fulfill pollen-specific requirements for actin dynamics. Real-time visualization of single filaments showed that ADF7 exhibits filament severing activity, which was verified in vivo by demonstrating that the average filament severing frequency was significantly decreased in *adf7* pollen tubes. The most compelling evidence supporting the importance of the severing activity comes from results showing that an ADF7-EGFP (for enhanced GFP) fusion protein deficient in severing activity that retains G-actin binding cannot complement *adf7*. Thus, we provide direct evidence that ADF-mediated severing regulates the turnover of longitudinal actin cables to promote pollen tube tip growth.

RESULTS

Loss of *ADF7* Increases Bundling of Actin Filaments in the Shanks of Pollen Tubes

To dissect the in vivo functions of *ADF7*, a T-DNA insertion line (Salk_024576; *adf7*) was analyzed (Figure 1A). No *ADF7* transcript was detected in *adf7* plants (Figure 1B), suggesting that the allele is a knockout. Pollen germination and tube elongation were initially assayed to determine the effects of loss of *ADF7*. Although pollen germination was not affected in *adf7* (see Supplemental Figure 1 online), the pollen tube elongation rate was significantly decreased in *adf7* compared with that of the wild-type Columbia-0 (Col-0) line (Figure 1C). Pollen tube elongation was fully rescued in the gADF7;*adf7* line (Figure 1D), suggesting that this phenotype is indeed caused by loss of *ADF7*. Thus, these data suggest that loss of *ADF7* has no overt effect on pollen germination but inhibits tube elongation.

We next sought to determine whether loss of *ADF7* affects the organization and dynamics of the actin cytoskeleton in the pollen tube. Pollen tubes derived from wild-type and *adf7* plants were subjected to F-actin staining with Alexa-488 phalloidin. No overt defects in actin organization were detected in *adf7* pollen tubes (Figure 1Eb) compared with wild-type pollen tubes (Figure 1Ea). However, we did note that the fluorescence associated with F-actin staining was brighter in *adf7* pollen tubes (Figure 1Ed) compared with wild-type pollen tubes (Figure 1Ec). To quantitatively analyze this phenotype, we focused on the shank region and subapical region because the F-actin staining in shank region was quite uniform in both wild-type and *adf7* pollen tubes (Figure 1E) and because ADF was implicated in regulating the construction of actin structures in subapical regions (Chen et al., 2002; Lovy-Wheeler et al., 2006). Analysis of the distribution of fluorescence pixel intensities revealed that larger intensity values were more frequent in *adf7* pollen tubes compared with wild-type pollen tubes (Figure 1F). Consequently, the average

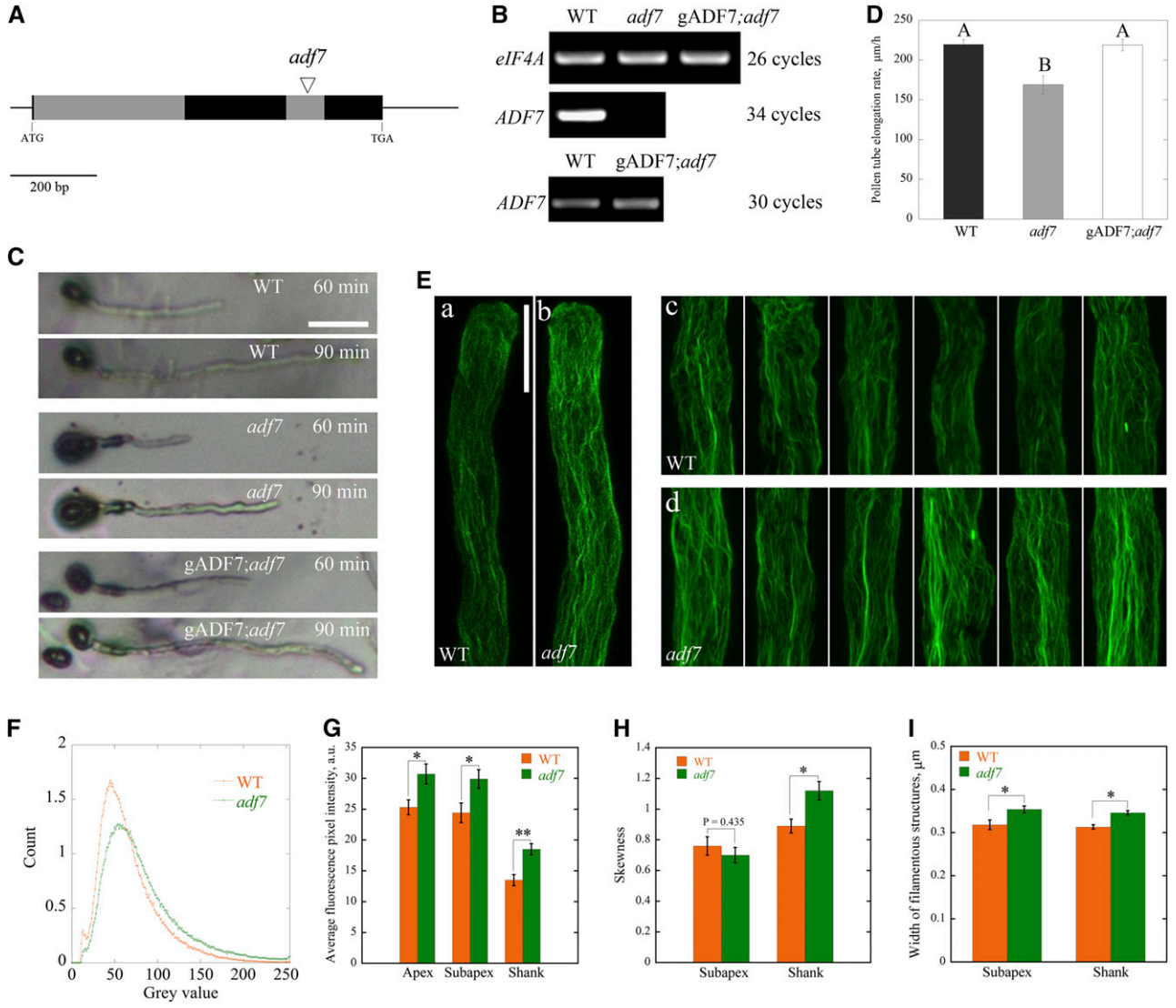

Figure 1. Loss of *ADF7* Increases the Amount of Filamentous Actin and Inhibits Pollen Tube Growth.

(A) Structure of the *ADF7* gene. *ADF7* contains three exons and two introns, which are indicated by black boxes and lines, respectively. Salk_024576 was inserted in the second intron to produce the *adf7* allele.

(B) *adf7* is a knockout allele. No *ADF7* transcripts were detected in *adf7* plants; however, *ADF7* expression was restored in the gADF7;*adf7* line. *eIF4A* served as the internal control. The number of cycles used to amplify PCR fragments is indicated in the figure. WT, the wild type.

(C) Pollen tube growth was inhibited in *adf7* plants. Individual pollen tubes derived from wild-type, *adf7*, and gADF7;*adf7* plants are shown at 60 and 90 min after germination. Bar = 50 μm.

(D) The pollen tube elongation rate was significantly decreased in *adf7* plants. Significant differences were assessed via a one-way analysis of variance, followed by an LSD post-hoc multiple comparison test. Values represent mean ± SE. Different capital letters indicate significant differences ($P < 0.01$). The experiment was repeated five times.

(E) No overt defect in the overall organization of actin filaments was detected in *adf7* pollen tubes, although more prominent actin cables were present in *adf7* pollen tubes. Representative images show wild-type **(a)** and *adf7* **(b)** pollen tubes and the shank regions of five representative wild-type **(c)** and *adf7* **(d)** pollen tubes. Images are the projections from all optical sections throughout pollen tubes. Bar = 10 μm.

(F) Fluorescence pixel intensity distribution of F-actin staining spanning the length of the pollen tubes. The percentage of fluorescent pixels with higher gray values was increased in *adf7* pollen tubes.

(G) The amount of F-actin was increased in *adf7* pollen tubes. The relative amount of F-actin was quantified by measuring the fluorescence pixel intensity in the apexes, subapexes, and shanks of pollen tubes. The definition for these regions is described in the methods section. Values represent mean ± SE. *$P < 0.05$ and **$P < 0.01$ by a Student's *t* test.

(H) The skewness of actin filaments increased in the shanks of *adf7* pollen tubes. Values represent mean ± SE. *$P < 0.05$ by a Student's *t* test.

(I) The width of filamentous structures increased in the shanks and subapexes of *adf7* pollen tubes. Values represent mean ± SE. *$P < 0.05$ by a Student's *t* test.

fluorescence pixel intensity was significantly increased in the shanks and subapexes of *adf7* pollen tubes compared with that of wild-type pollen tubes (Figure 1G). Since phalloidin specifically binds to F-actin (Cooper, 1987), fluorescence intensity is positively correlated with the amount of F-actin. Thus, the data suggest that loss of *ADF7* increases the amount of F-actin. Furthermore, measurement of skewness revealed that these values were significantly increased in *adf7* pollen tubes (Figure 1H), along with the measurement showed that the average width of filamentous structures increased in *adf7* pollen tubes (Figure 1I), suggesting that the extent of filament bundling was increased in *adf7* pollen tubes. However, no overt differences were observed in the organization or amount of F-actin in pollen grains from *adf7* plants compared with wild-type plants (see Supplemental Figure 2 online). Thus, these results suggest that ADF7 regulates pollen tube growth by promoting disassembly of actin filaments.

Loss of *ADF7* Renders Pollen Germination and Tube Elongation Resistant to Latrunculin B

We next examined whether the organization and dynamics of actin filaments were differentially affected by actin-targeted drugs in *adf7* pollen. We approached this question by analyzing the effects of the actin monomer sequestering agent latrunculin B (LatB) (Coué et al., 1987; Gibbon et al., 1999) on pollen germination and tube growth. Results from this analysis revealed that germination of *adf7* pollen was resistant to treatment with 3 nM LatB compared with both wild-type and gADF7;*adf7* pollen (Figure 2A; see Supplemental Figure 3 online). Further analysis of a series of LatB concentrations further confirmed that the germination of *adf7* pollen was resistant to LatB (Figure 2B). This phenotype was fully reversed in gADF7;*adf7* plants (Figure 2B). Because 3 nM LatB was previously shown to result in half-maximum growth inhibition of wild-type *Arabidopsis* pollen tubes (Zhang et al., 2010) and was associated with LatB resistance in *adf7* plants, two LatB concentrations (3 and 10 nM) were selected for further analysis of the effects of LatB on *adf7* pollen tube elongation. The average pollen tube elongation rates for wild-type (202.1 ± 8.5 μm/h; $n = 3$; mean ± SE) and *adf7* (159.6 ± 6.2 μm/h; $n = 3$) plants were normalized to 100%. Addition of 3 and 10 nM LatB to standard germination medium (GM) reduced pollen tube elongation rates to 41.4% ± 3.7% ($n = 3$) and 25.7% ± 1.5% ($n = 3$) for wild-type pollen tubes and 90.7% ± 1.7% ($n = 3$) and 59.7% ± 7.3% ($n = 3$) for *adf7* pollen tubes, respectively (Figure 2C). Thus, these data suggest that loss of *ADF7* renders both pollen germination and tube elongation resistant to LatB.

The Actin Cytoskeleton in *adf7* Pollen Grains Is Resistant to Perturbation by LatB

We next visualized the effect of LatB on the actin cytoskeleton of the pollen grain, since it has been shown to be a good experimental system for visualization of actin filaments and quantification of F-actin (Huang et al., 2006; Ye et al., 2009; Zhang et al., 2010). Pollen grains were stained with Alexa-488 phalloidin after treatment with 200 nM LatB for 30 min. Actin filaments became fragmented in both wild-type and *adf7* pollen grains treated with LatB and were less abundant compared with untreated wild-type and *adf7* pollen grains (Figure 2D), consistent with previous reports demonstrating net actin depolymerization induced by LatB (Gibbon et al., 1999; Snowman et al., 2002; Zhang et al., 2010). However, actin filaments in *adf7* pollen grains appeared brighter than those of wild-type pollen grains after LatB treatment (Figure 2D). To assess this difference, the relative amount of F-actin was quantified by measuring the average fluorescence pixel intensity associated with F-actin staining as described previously (Ye et al., 2009; Zhang et al., 2010). The amount of F-actin in untreated wild-type and *adf7* pollen grains was normalized to 100%. The relative amount (mean ± SE) of F-actin was determined to be 41.0% ± 5.0% ($n = 3$) and 80.6% ± 4.2% ($n = 3$) for LatB treated wild-type and *adf7* pollen grains, respectively (Figure 2E). These observations suggest that loss of *ADF7* results in stabilization of actin filaments, implicating ADF7 in promotion of actin turnover.

ADF7 Depolymerizes and Severs Actin Filaments, but to a Lesser Degree Than ADF1

To determine the biochemical basis for the function of ADF7, recombinant ADF7 was produced (Figure 3A, lane 1), and its activity was compared with the well-characterized ADF1 protein (Figure 3A, lane 2; Carlier et al., 1997). Although some ADF/cofilins have been shown to bind ADP-G-actin and ATP-G-actin with equal affinity, such as chicken ADF and mouse cofilin-2 (Vartiainen et al., 2002; Chen et al., 2004), most ADF/cofilins have been shown to prefer ADP-G-actin over ATP-G-actin (Maciver and Hussey, 2002; Bamburg and Bernstein, 2008). ADF7 quenched the fluorescence of both 7-chloro-4-nitrobenzo-2-oxa-1,3-diazole (NBD)-ADP-G-actin and NBD-ATP-G-actin, but to a lesser degree than ADF1 (Figures 3B and 3C; see Supplemental Table 1 online). Similar to ADF1, ADF7 preferentially bound ADP-actin (see Supplemental Table 1 online). ADF7 also inhibited nucleotide exchange on ADP-G-actin under physiological conditions, but this activity was less potent than that of ADF1 (Figure 3D). These data suggest that ADF7 is a typical ADF. As expected, it promotes actin depolymerization (Figure 3E; see Supplemental Figure 4A online) and enhances the actin turnover rate (Figure 3F). However, these effects were weaker than those of ADF1.

The depolymerizing activity of ADF7 was further confirmed by visualizing its effect on shortening of actin filaments (Figures 3Gb and 3Gc). ADF7 reduced the length of actin filaments in a dose-dependent manner, but to a lesser degree than ADF1 (Figure 3Ge). To distinguish whether the filament shortening effect was a result of monomer dissociation, filament severing, or both, we directly visualized single filaments using time-lapse total internal reflection fluorescence (TIRF) microscopy. In the absence of ADF proteins, few breaks were observed along actin filaments (Figure 3Ha; see Supplemental Movie 1 and Supplemental Movie Legends 1 online). By contrast, the addition of ADF7 resulted in increased filament breakage (Figure 3Hb; see Supplemental Movie 2 online). Both ADF7 and ADF1 severed filaments in a dose-dependent manner, although ADF7 was less effective than ADF1 (Figure 3Hc). We also measured monomer off-rate in the absence or presence of ADF proteins and found that both ADF7 and ADF1 enhanced monomer dissociation from the pointed ends of actin filaments (see Supplemental Figure 4B online). Again, ADF7 was less efficient

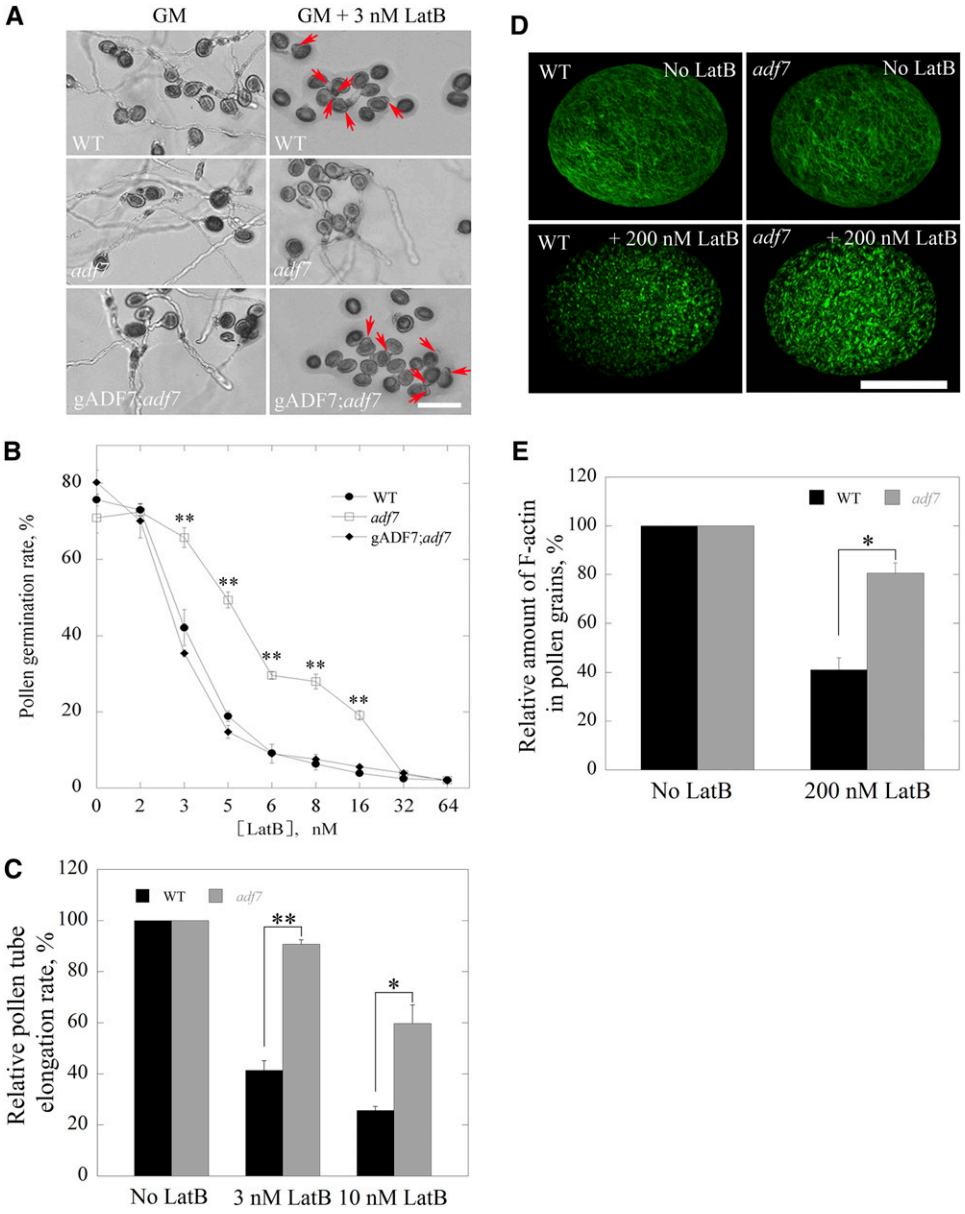

Figure 2. Loss of *ADF7* Inhibits Actin Turnover.

(A) Loss of *ADF7* renders pollen germination resistant to LatB. Pollen grains derived from wild-type (WT), *adf7*, and gADF7;*adf7* plants were germinated in standard GM for 3 h in the presence or absence of 3 nM LatB. Red arrows indicate the pollen tube protrusion sites. Bar = 50 μm.

(B) Loss of *ADF7* renders pollen germination resistant to a range of LatB concentrations. Values represent mean ± SE. **P < 0.01 by a Student's *t* test.

(C) Pollen tube elongation in *adf7* plants is resistant to LatB. The average pollen tube elongation rate in standard GM was normalized to 100% for the wild type and *adf7*. The relative pollen tube elongation rate for wild-type and *adf7* pollen tubes treated with 3 or 10 nM LatB were subsequently normalized to their untreated controls. The experiment was repeated three times. Values represent mean ± SE. *P < 0.05 and **P < 0.01 by a Student's *t* test.

(D) The actin cytoskeleton of *adf7* pollen is resistant to LatB. Pollen grains derived from the wild type and *adf7* were subjected to treatment with 200 nM LatB for 30 min, followed by staining with Alexa-488 phalloidin. Images are the projections from all optical sections throughout the whole pollen grains. Bar = 10 μm.

(E) Quantification of the relative amount of F-actin in pollen grains. The amount of F-actin fluorescence presents prior to LatB treatment was normalized to 100% for the wild type and *adf7*. Values represent mean ± SE. **P < 0.01 by a Student's *t* test.

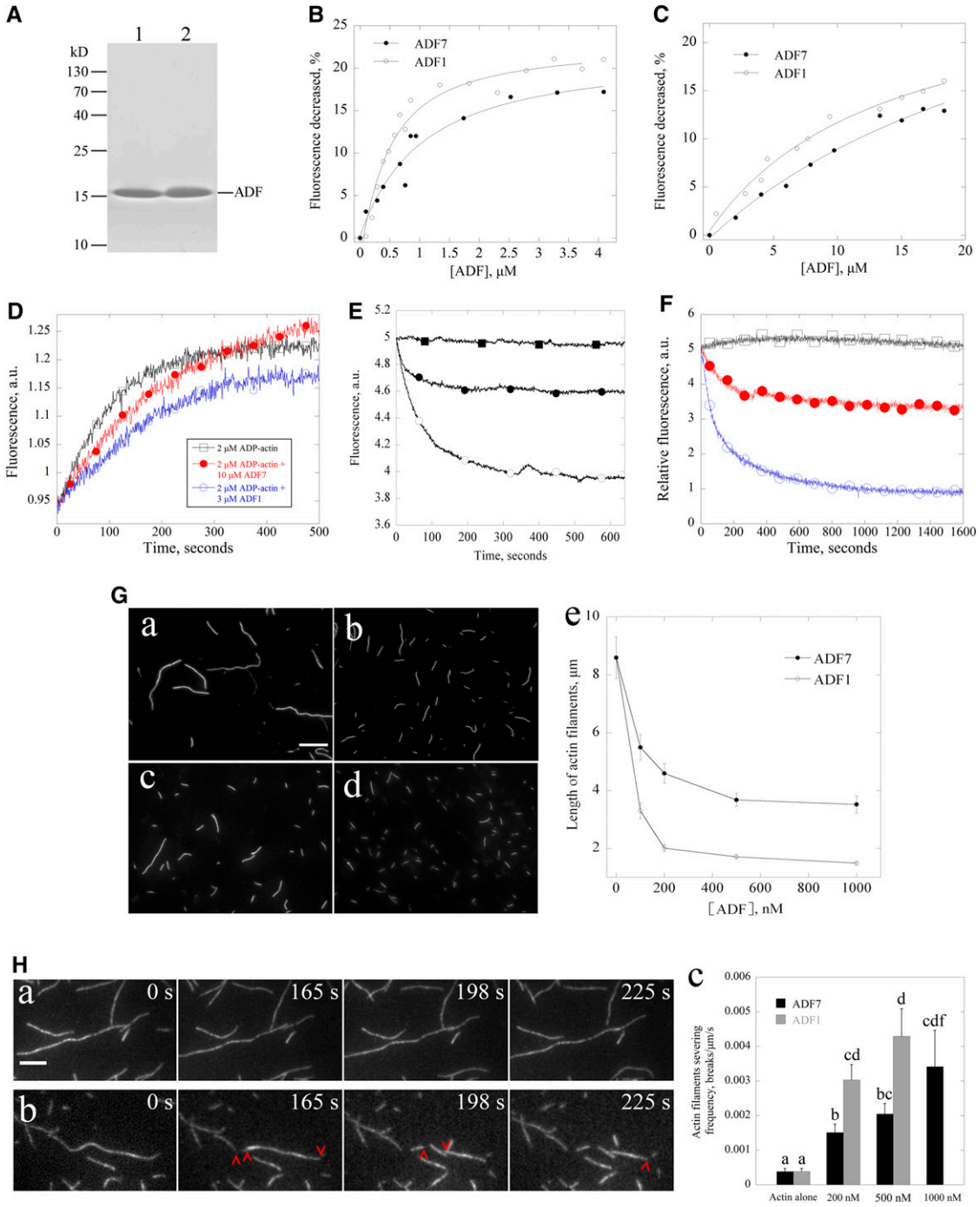

Figure 3. ADF7 Is a Typical ADF but Is less Efficient Than ADF1.

(A) SDS-PAGE analysis of purified recombinant ADF proteins. Lane 1, ADF7; lane 2, ADF1.
(B) and **(C)** ADF7 has weaker binding affinity for both ADP-G-actin **(B)** and ATP-G-actin **(C)** than ADF1 at pH 8.0. NBD-ADP-G-actin or NBD-ATP-G-actin (0.2 μM) was incubated with increasing concentrations of ADF7 or ADF1 for 1 min, and the changes in NBD fluorescence were monitored. The relative decrease in fluorescence over time was plotted. Dissociation constants (K_d) values were calculated by fitting the data to Equations 1 to 3 in Methods. K_d values for ADF7 and ADF1 binding to ADP-G-actin and ATP-G-actin were determined to be 0.92 and 0.38 μM **(B)**, and 29.6 and 13.7 μM **(C)**, respectively.
(D) ADF7 inhibits nucleotide exchange on ADP-G-actin in the presence of 20 mM Tris-HCl, pH 8.0, and 50 mM NaCl, but to a lesser degree than ADF1. a.u., arbitrary units.

than ADF1 (see Supplemental Figure 4B online). Thus, these data suggest that ADF7 is a typical ADF but that its activity is weaker than that of ADF1.

ADF7 Decorates Actin Cables in the Shanks of Pollen Tubes

To determine where ADF7 is localized to the pollen tube, we generated N-terminal, C-terminal, and several intramolecular ADF7-EGFP fusion constructs according to published methods (Okreglak and Drubin, 2007; Bou Daher et al., 2011). Expression of these constructs was driven by the native *ADF7* promoter. *ADF7* transcript levels were restored in transgenic plants carrying each of the different GFP fusion constructs (see Supplemental Figure 5B online). Among these lines, only gADF7-EGFP$_{V10}$;*adf7* fully rescued the LatB-resistant germination and tube elongation phenotypes (see Supplemental Figures 5C and 5D online), indicating that ADF7-EGFP$_{V10}$ is functional and faithfully represents the subcellular localization of ADF7 in pollen. ADF7-EGFP$_{V10}$ decorated actin filaments throughout the pollen grain (Figure 4A). In pollen tubes of different lengths, it primarily decorated actin cables in the shank region (Figures 4B to 4D), and the GFP signal was quite dim in the apical and subapical regions (Figures 4B to 4D). We also examined the subcellular distribution patterns of other ADF7-EGFP fusion proteins, revealing that these proteins did not localize to obvious filamentous structures in either pollen grains or tubes (see Supplemental Figure 5E online). Together, these data suggest that ADF7 decorates longitudinal actin cables in pollen tubes.

ADF7 Promotes Turnover of Single Actin Filaments in the Shanks and Subapexes of Pollen Tubes

To explore the mechanism by which ADF7 regulates the dynamics of longitudinal actin cables in the pollen tube, actin filaments were labeled with EGFP-lifeact, which has previously been shown to decorate actin filaments in the pollen tube (Qu et al., 2013; Zhu et al., 2013). To determine the underlying changes in single actin filaments dynamics, we initially wanted to define the properties for single actin filaments by determining their fluorescence pixel intensities and widths. We found that the fluorescence pixel intensity positively correlates with the width for all measured filaments, and some filamentous structures with smaller intensity values form a population with the intensity peak at 960 (see Supplemental Figure 6 online). The filamentous structures within this population with intensity values below 1200 were assumed to be single filaments and were selected from *adf7* and wild-type pollen tubes for further analysis. Several dynamic parameters associated with single filaments were determined to see whether ADF7 contributes to the turnover of single filaments in shanks and subapexes. Filament severing (Figures 5Aa and 5Ba; see Supplemental Movies 3 and 4 online) and depolymerization (Figure 5Ab and 5Bb; see Supplemental Movies 5 and 6 online) events were traced and quantified. Severing frequency was significantly decreased in shanks and subapexes of *adf7* pollen tubes compared with that of wild-type pollen tubes (Figure 5C). Additionally, the depolymerization rate was significantly decreased in the shanks of *adf7* pollen tubes, whereas no obvious difference was detected in subapexes of *adf7* pollen tubes, compared with wild-type pollen tubes (Figure 5C). Consequently, the maximum filament lifetime significantly increased in shanks and subapexes of *adf7* pollen tubes, whereas no obvious difference was detected in maximum filament length of *adf7* pollen tubes, compared with wild-type pollen tubes (Figure 5C). Additionally, we found that the elongation rate of actin filaments was significantly decreased in the shanks of *adf7* pollen tubes, whereas no obvious difference was detected in the subapexes of *adf7* pollen tubes compared with wild-type pollen tubes (Figure 5C). At the moment, it is not clear why loss of ADF7 decreased the elongation rate of actin filaments in shanks. Previous results showed that loss of ADF4 has differential effects on actin elongation in the epidermal cells from 5-d-old seedlings and 11- and 13-d-old seedlings (Henty et al., 2011). Thus, these data suggest that ADF7 promotes actin turnover by severing filaments and promoting monomer dissociation.

Loss of *ADF7* Decreases Debundling Frequency

We next determined whether ADF7 contributes to the bundling and debundling events of actin filaments. We tried to trace the process of actin bundles formation and deformation. As shown in Figure 6A (see Supplemental Movie 7 online), two adjacent actin bundles were zipped together to generate the heavy bundle in wild-type pollen tubes, which was supported by the measurement showing that the fluorescence pixel intensity increased while they were zipped together (Figure 6B). We also noted that the heavy actin bundles can split into two small actin bundles (Figure 6C; see Supplemental Movie 8 online). We next quantified the parameters associated with actin bundles dynamics in shanks. Surprisingly, we found that no obvious difference in

Figure 3. (continued).

(E) ADF7 depolymerized actin filaments but was less potent than ADF1. Preassembled actin filaments (0.5 μM) were incubated with either 4 μM ADF7 or 4 μM ADF1 to induce actin depolymerization at pH 7.0. Actin depolymerization was monitored by measuring the changes in light scattering. Closed squares, 0.5 μM F-actin; closed circles, 0.5 μM F-actin + 4 μM ADF7; open circles, 0.5 μM F-actin + 4 μM ADF1. a.u., arbitrary units.

(F) ADF7 accelerates actin turnover but is less efficient than ADF1. The actin turnover rate was measured by analyzing the change in fluorescence of actin after exchange of ε-ATP for nonfluorescent ATP. Open squares, 4 μM εADP-actin filaments; closed red circles, 4 μM εADP-actin filaments + 5 μM ADF7; open circles, 4 μM εADP-actin filaments + 5 μM ADF1. a.u., arbitrary units.

(G) ADF7 reduces the lengths of actin filaments but to a lesser degree than ADF1. Actin alone **(a)**, F-actin + 200 nM ADF **(b)**, F-actin + 500 nM ADF7 **(c)**, and F-actin + 500 nM ADF1 **(d)**. Bar = 5 μm. Mean length of actin filaments versus ADF **(e)**. Values represent mean ± SE, $n = 3$.

(H) ADF7 is able to sever actin filaments, but is less efficient than ADF1. The left panel shows time-series images of actin filaments in the absence **(a)** or presence of 500 nM ADF7 **(b)** at pH 7.0. Red arrows indicate filament severing events. Bar = 5 μm. ADF7 is less efficient than ADF1 at severing actin filaments **(c)**. Values represent mean ± SE; $n = 3$. Lowercase letters indicate difference at $^{**}P < 0.01$ by a Student's t test.

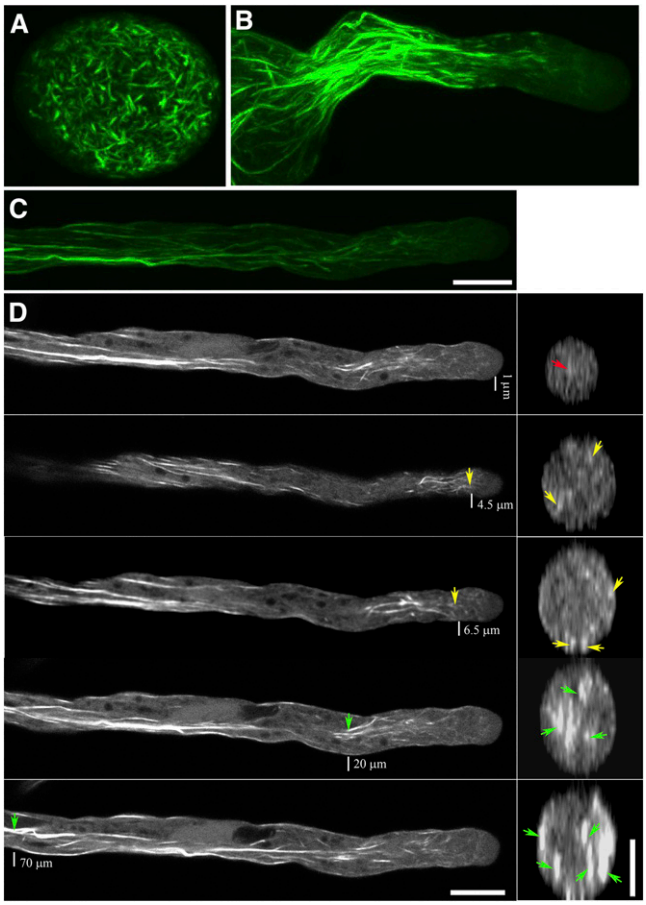

Figure 4. ADF7-EGFP$_{V10}$ Decorates Filamentous Structures in Pollen Grains and Tubes.

gADF7-EGFP$_{V10}$;*adf7* fluorescence was visualized in pollen grain and tubes.

(A) ADF7 decorates actin filaments throughout the pollen grain.

(B) and **(C)** ADF7 primarily decorates longitudinal actin cables within pollen tubes. Images in **(A)** to **(C)** are the maximum projections of all optical sections. Bar = 10 μm for **(A)** to **(C)**.

(D) Four longitudinal optical sections for the pollen tube shown in **(C)** are displayed in left panel. The right panel shows the transverse sections of pollen tube taken at the position indicated by the white lines at specific distances from the tip. Different colored arrows indicate the decorated filamentous structures at the indicated positions. Bar = 10 μm in the left panel and 5 μm in the right panel.

bundling frequency was detected in *adf7* pollen tubes, whereas debundling frequency significantly decreased in *adf7* pollen tubes compared with wild-type pollen tubes (Figure 6D). Therefore, the decrease in debundling frequency may at least partially account for the increase in the extent of filament bundling in *adf7* pollen tubes.

The Severing Activity of ADF7 Is Vital for Its Function in Vivo

Considering that ADF7-EGFP fusion proteins act differentially in vivo, careful documentation of their biochemical activities in combination with meaningful comparisons can provide insight into specific mechanisms of action of ADF7 in vivo. In addition to ADF7-EGFP$_{V10}$, we selected another intramolecular fusion protein, ADF7-EGFP$_{D75}$, to perform the in vitro biochemical analysis (see Supplemental Figure 7A online). Results from F-actin high-speed cosedimentation experiments revealed that glutathione *S*-transferase (GST)-ADF7-EGFP$_{V10}$ binds to F-actin better than GST-ADF7-EGFP$_{D75}$ (see Supplemental Figures 7B and 7C online). The 6His-ADF7-EGFP$_{V10}$ fusion protein had slightly less severing activity than ADF7, although no significant difference was detected (see Supplemental Figure 7D online). By contrast, no severing activity was detected for 6His-ADF7-EGFP$_{D75}$ (see Supplemental Figure 7D online). However, both 6His-ADF7-muEGFP$_{V10}$ and 6His-ADF7-muEGFP$_{D75}$ bind G-actin as well as ADF7 (see Supplemental Figure 7E online). Thus, these data suggest that ADF7-EGFP$_{V10}$ retains levels of filament severing and G-actin binding activity comparable to the wild-type protein. By contrast, though ADF7-EGFP$_{D75}$ retains G-actin binding activity, it is deficient in filament severing. Therefore, our data provide compelling evidence that the severing activity of ADF7 is vital for its function in vivo.

DISCUSSION

ADF7-Mediated Actin Dynamics Are Required for Pollen Tube Growth

ADF has been shown to be crucial for the growth of several types of tip growing cells, including moss protonemal cells (Augustine et al., 2008) and root hairs (Dong et al., 2001). ADF has also been implicated in pollen tube growth, primarily due to results from gain-of-function studies (Chen et al., 2002; Li et al., 2010). Here, we found that loss of function of a pollen-specific *Arabidopsis* ADF isovariant, *ADF7*, inhibits pollen tube growth (Figure 1C). The effect of loss of function of *ADF7* on tip growth is similar to that of loss of function of *ADF* on moss protonemal cell growth (Augustine et al., 2008) but differs from a study showing that downregulation of *ADF1* promotes root hair growth (Dong et al., 2001). Loss of *ADF7* increased the amount of actin filaments in pollen tubes (Figure 1E), similar to the reported functions of *ADF1*, *ADF2*, *ADF4*, and moss ADF (Dong et al., 2001; Augustine et al., 2008; Clément et al., 2009; Henty et al., 2011). These observations suggest that increases in the amount of filamentous actin induced by downregulation of *ADF* are a common phenomenon, consistent with a role for ADF in depolymerizing actin filaments. On the other hand, these results also indicate that the net increase in the amount of filamentous actin resulting from *ADF* loss of function has differential effects on the growth of various types of tip growing cells, suggesting that the relationship between ADF-mediated actin dynamics and tip growth requires further characterization.

The effect of *ADF* loss of function on actin filament bundling is very likely indirect and is probably due to a decrease in the rate of single actin filament turnover. A previous study showed that single actin filament dynamics are dominated by prolific severing events that balance rapid polymerization (Staiger et al., 2009). ADF was verified as an important player in the stochastic dynamics

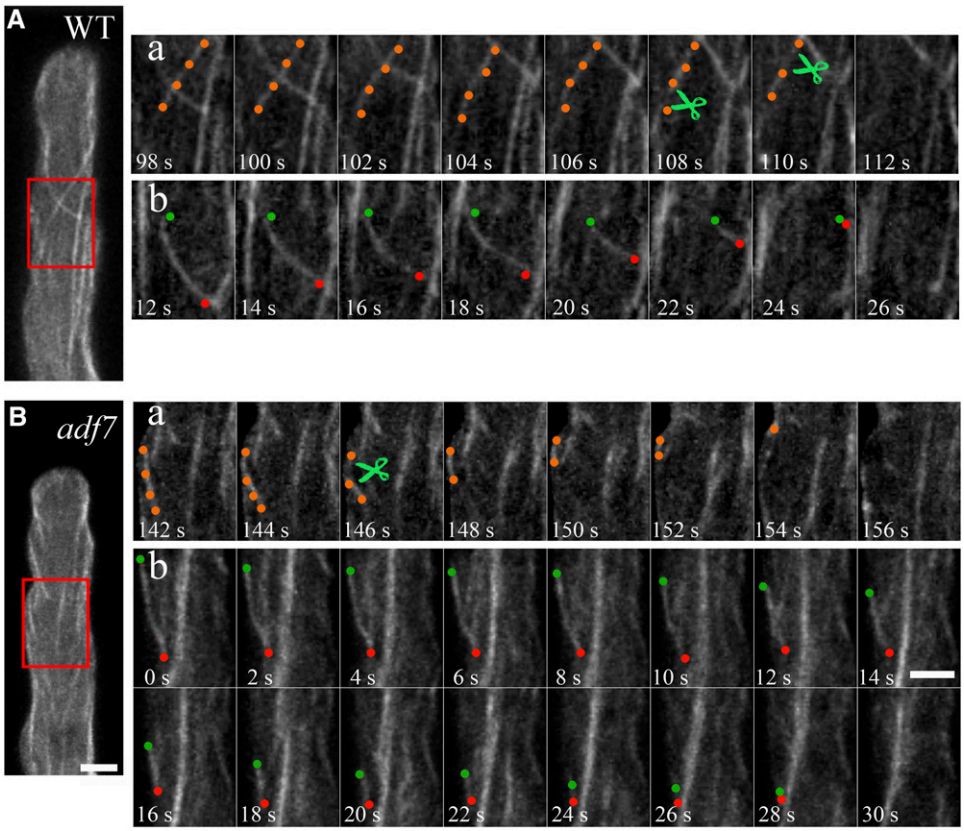

C

Stochastic dynamic parameters	WT		*adf7*	
	Shank	Subapex	Shank	Subapex
Severing frequency (breaks/μm/s)	0.020 ± 0.002 (51)	0.024 ± 0.005 (27)	0.014 ± 0.002 (40)*	0.013 ± 0.003 (24)*
Depolymerization rate (μm/s)	0.334 ± 0.022(36)	0.204 ± 0.01 (30)	0.271 ± 0.015 (27)*	0.225 ± 0.012 (24)ND
Max filament length (μm)	4.63 ± 0.25 (55)	3.277 ± 0.322 (30)	4.79 ± 0.29 (44)ND	3.704 ± 0.213 (35)ND
Max filament life time (s)	25.7 ± 1.2 (37)	25.4 ± 1.73 (30)	32 ± 2.0 (32)*	31.6 ± 1.94 (28)*
Elongation rate (μm/s)	0.430 ± 0.021 (25)	0.245 ± 0.02 (24)	0.313 ± 0.135 (25)**	0.271 ± 0.014 (27)ND

Figure 5. Time-Lapse Imaging of Actin Filaments Revealed a Reduction in the Severing Frequency in *adf7* Pollen Tubes.

Three-dimensional time-lapse spinning disk confocal microscopy was used to image actin filaments in pollen tubes expressing Lat52: *EGFP-Lifeact*. Pollen tubes with an average length of ~200 μm were selected for imaging. Bars = 3 μm for images in **(A)** and **(B)**.

(A) Dynamics of single actin filaments in the shank of a wild-type (WT) pollen tube. The image presented is an optical section. The right panels show an enlarged view of the region from shank in the red box. **(a)** A filament highlighted with orange dots underwent severing, and the green scissors indicate the severing events. See Supplemental Movie 3 online for the entire series. **(b)** Red and green dots indicate the ends of a filament that underwent shrinkage. The image was from the same region as that in **(a)** but in a different optical section. See Supplemental Movie 5 online for the entire series.

(B) Dynamics of single actin filaments in the shank of an *adf7* pollen tube. The image presented is an optical section. **(a)** A filament highlighted with orange dots underwent severing, and the green scissors indicate a severing event. The image corresponds to the red boxed region in the left panel. See Supplemental Movie 4 online for the entire series. **(b)** Red and green dots indicate the ends of a single filament that underwent shrinkage. See Supplemental Movie 6 online for the entire series.

(C) Quantification of parameters associated with single actin dynamics in wild-type and *adf7* pollen tubes. Actin filaments from the shanks and subapexes were analyzed. More than 27 pollen tubes from the wild type and *adf7* were used. Values given are means ± SE. ND, no significant difference; *P < 0.05 and **P < 0.01 by a Student's *t* test.

model (Henty et al., 2011). Consistent with a role for ADF7 in this process, we demonstrated that the average severing frequency was significantly decreased in *adf7* pollen tubes (Figure 5C), while the lifetime and maximum filament length of single actin filaments were significantly increased (Figure 5C). These parameters may therefore increase the probability of single actin filaments being brought together by bundling factors, such as villins, fimbrins, LIMs, and formins, among others (Thomas et al., 2009; Thomas, 2012). Certainly, it may also be possible that ADF7 directly competes for filament side binding with bundling factors.

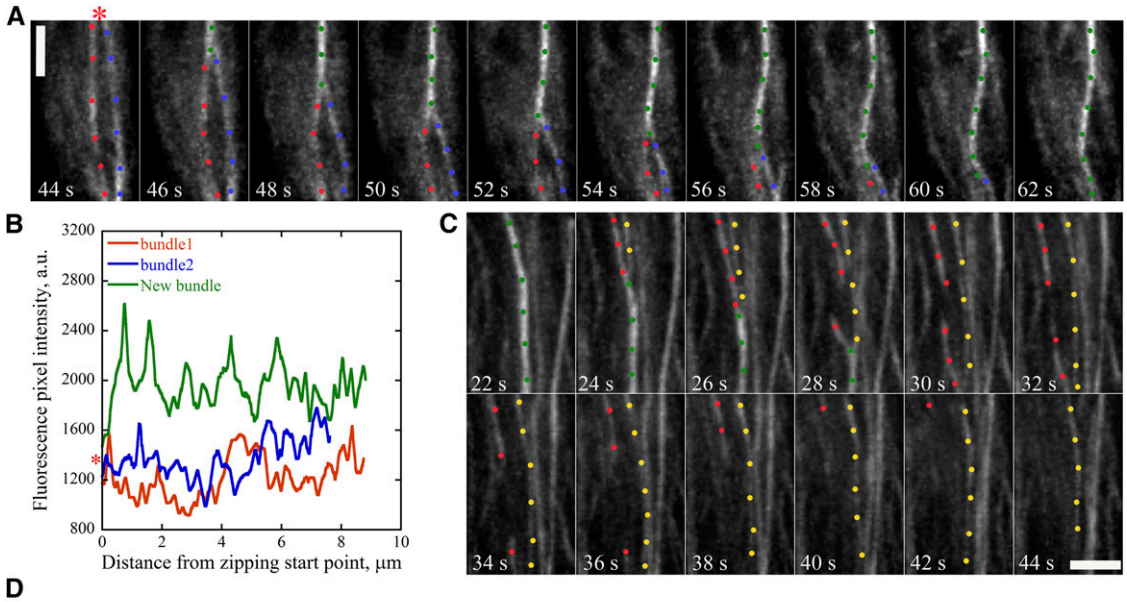

D

Bundle formation / deformation frequency	WT	*adf7*
Bundling frequency (events/μm^2/s)	0.00023 ± 5.4×10^{-5} (24)	0.00031 ± 4.2×10^{-5} (21) ND
Debundling frequency (events/μm^2/s)	0.00054 ± 6.5×10^{-5} (29)	0.00023 ± 4.9×10^{-5} (23) **

Figure 6. The Frequency of Debundling Is Significantly Decreased in *adf7* Pollen Tubes.

To analyze the bundling and debundling events in the shanks of pollen tubes, a 6 × 10-μm^2 region that was 20 μm away from the tip was selected.
(A) The time-lapse process showing that two thin actin bundles form a think actin bundle by zipping in a wild-type pollen tube. Red and blue dots indicate two original thin actin bundles, and green dots indicate the newly generated thick actin bundles. Red asterisk indicates the start point of zipping. Bar = 3 μm. See Supplemental Movie 7 online for the entire series.
(B) Measurement of the fluorescence pixel intensity of two original thin actin bundles and the new generated thick actin bundles. The fluorescence pixel intensity was measured at 44 s for both thin actin bundles and at 62 s for the thick actin bundles. a.u., arbitrary units.
(C) The time-series images indicate the process of debundling. Green dots indicate the original thick bundle, and red and yellow dots indicated two generate thin filamentous structures via debundling. Bar = 3 μm. See Supplemental Movie 8 online for the entire series.
(D) Debundling frequency significantly decreased in *adf7* pollen tubes. More than 20 bundles from 10 pollen tubes were measured for both the wild type (WT) and *adf7*. Values represent mean ± SE; ND, no significant difference; **P < 0.01 by a Student's *t* test.

This is very likely the case, since ADF is a very abundant protein (Chaudhry et al., 2007) and mainly associates with filaments in the pollen tube (Figure 4; discussed below). In support of this hypothesis, an elegant study from fission yeast showed that cofilin selectively competes with bundling factors for binding of actin filaments (Skau and Kovar, 2010). Therefore, it could be possible that loss of ADF7 increased the binding of bundling factors to filaments to consequently increase the extent of filament bundling (Figure 1). Meanwhile, the increase in binding of bundling factors may impact the physical properties of actin bundles. The decrease in debundling frequency in *adf7* pollen tubes, to some extent, supports this (Figure 6).

Different mechanisms have been envisioned to understand the role of the actin cytoskeleton in pollen tube growth. In early days, the actin cytoskeleton was simply viewed as providing tracks for delivery of secretory vesicles containing materials necessary for membrane extension and cell wall synthesis to the tip (Taylor and Hepler, 1997; Kost et al., 1998). In this model, alterations in the actin-bundling status in *adf7* pollen tubes (Figure 1E) could matter for actin's role as a molecular track for myosin motors. However, based on findings demonstrating that an extremely dynamic population of actin filaments is present at the apical region that is crucial for pollen tube growth (Lin and Yang, 1997; Gibbon et al., 1999; Geitmann et al., 2000; Vidali et al., 2001; Qu et al., 2013) and root hair growth (Miller et al., 1999), it is possible that ADF could be involved in regulation of actin dynamics at pollen tube tips, though it has been assumed to be inactive within this region (Allwood et al., 2001).

The role of the actin cytoskeleton in epidermal cell expansion is not well understood either. Parameters associated with single filament dynamics in growing hypocotyl epidermal cells have been shown to be similar to that of nongrowing hypocotyl epidermal cells (Staiger et al., 2009), implying that actin dynamics may not be directly coupled with cell elongation. In support of this, actin polymerization was favored in different types of cells but had opposite effects on the growth of cotyledon petiole cells and hypocotyl epidermal cells from *adf4* plants (Henty et al., 2011). These observations also suggest that the relationship between filament bundling status and cell elongation might be organ, tissue, or cell type specific. Further supporting evidence

comes from a study showing that loss of function of *VILLIN2* and *VILLIN3* has different effects on the elongation of epidermal and interfascicular fiber cells (Bao et al., 2012; van der Honing et al., 2012). Henty et al. (2011) divided actin filaments into two populations in cells, comprising stable actin bundles and dynamic single actin filaments, and proposed that the ratio of single actin filaments to bundles is important for cell expansion. This may also apply to the pollen tube regarding the action mechanisms of the actin cytoskeleton, in which ADF7 may play an important role in the dynamic conversion between these two populations of actin filaments.

Severing Is the Key Mechanism Underlying ADF-Mediated Regulation of Actin Dynamics in Pollen Tubes

ADF/cofilin has been shown to be an important regulator of actin turnover among organisms (Bernstein and Bamburg, 2010). Consistent with this role, the actin turnover rate was decreased in *adf7* pollen (Figures 2D and 2E). However, the molecular mechanisms underlying the regulation of actin turnover by ADF/cofilin remain quite controversial. Historically, ADF/cofilin was thought to depolymerize actin filaments by promoting dissociation of actin monomers from the pointed end, primarily based on results from in vitro biochemical characterization of *Arabidopsis* ADF1 (Carlier et al., 1997). However, direct visualization of the effects of ADF/cofilin on single actin filament dynamics has shown that filament severing is the primary mechanism by which ADF/cofilins promote actin filament turnover (Andrianantoandro and Pollard, 2006; Chan et al., 2009; Henty et al., 2011; Suarez et al., 2011; Shi et al., 2013). In support of this mechanism, mathematic modeling results based on the biochemical activity of ADF/cofilins also indicate that depolymerization alone cannot account for the rates of actin turnover mediated by ADF/cofilin in vitro (Roland et al., 2008; Berro et al., 2010; Kueh et al., 2010). Direct visualization of single filament dynamics in vivo have indeed verified that ADF/cofilin contributes to filament severing (Henty et al., 2011). Specific abolishment of the severing activity of cofilin through specific point mutations suggests that the severing activity of cofilin is essential (Chen and Pollard, 2011). However, to date, no similar study has been reported in plants.

As ADF7 exhibits reasonable levels of filament severing activity in biochemical assays (Figure 3; discussed below), we propose that the filament severing activity of ADF7 is important for its role in regulating cellular actin dynamics. Consistent with this hypothesis, we demonstrated that loss of *ADF7* significantly decreases the average severing frequency in pollen tubes (Figure 5C). Furthermore, we showed that an ADF7-EGFP fusion protein defective in severing activity that retains G-actin binding cannot rescue *adf7*-associated phenotypes (see Supplemental Figures 5 and 7 online). Thus, these data suggest that severing activity is essential for the function of ADF7 in pollen tubes. Our data showed that the average severing frequency decreased in the subapical region as well (Figure 5C). Considering that ADF7 also decorates filamentous structures in subapical regions of pollen tubes, though it is less abundant compared with that in the shank (Figures 4C and 4D), the effect is unlikely indirect. It was assumed that ADF participates in the construction of actin collars via severing filaments to generate more ends to boost polymerization via elongation and therefore build the prominent collar structures (Lovy-Wheeler et al., 2006). If ADF7 contributes to the construction of actin collars via this manner, it was expected that the formation of actin collars will somehow be compromised. However, the actin collar structures became more prominent in *adf7* pollen tubes (Figures 1E and 1G to 1I), suggesting that we cannot simply fit the function of ADF7 to the previous model (Lovy-Wheeler et al., 2006). Nonetheless, our data suggest that ADF7 plays a role in promoting the turnover of actin filaments within actin collars. Certainly, it could be possible that other ADF isovariants, such as ADF10, may play distinct roles from ADF7 in the construction of actin collars.

ADF7 Decorates Actin Cables in the Pollen Tube

Considering that both *ADF7* and *ADF10* are expressed in mature pollen at roughly similar high levels (Honys and Twell, 2003; Pina et al., 2005) and multiple actin arrays are present in pollen tubes (Cheung and Wu, 2008; Chen et al., 2009; Staiger et al., 2010), the question is raised whether a particular ADF isovariant regulates distinct actin arrays and/or multiple ADF isovariants coordinately regulate a particular actin array. One key piece of information needed to answer this question is determination of the precise subcellular localization of each ADF isovariant. Because different pollen ADFs share high amino acid sequence identity with one another (Lopez et al., 1996), generation of isovariant-specific antibodies for immunostaining is problematic. Therefore, fluorescent protein tagging needs to become the strategy of choice to tackle this issue. However, since ADF is a small protein, either N- or C-terminal fusions may alter protein function. Indeed, fusion constructs containing cofilin with GFP fused either at its N or C terminus do not complement its loss of function phenotypes in budding yeast (Okreglak and Drubin, 2007). However, a previous study undertook a very wise strategy, creating a fusion construct with GFP located within cofilin, and found that this construct fully rescued cofilin loss of function (Okreglak and Drubin, 2007). These results suggest that this intramolecular GFP fusion minimally affects ADF/cofilin function and likely provides a faithful probe that represents the intracellular localization of the endogenous protein. However, the authors did not test the activity of this fusion protein biochemically. Bou Daher et al. (2011) undertook a similar strategy to make intramolecular GFP fusions for both ADF7 and ADF10, although GFP was inserted in a different region, and found that both GFP fusion proteins decorated actin filaments in pollen grains and tubes. However, the authors did not test whether these constructs were fully functional. Having a null mutant for *ADF7* in hand places us in the position to fully address this question. In addition to generating a construct with GFP fused at the same location as that of Bou Daher et al. (2011), we also made several additional intramolecular GFP fusion constructs with GFP fused near the region corresponding to the budding yeast cofilin fusion (Okreglak and Drubin, 2007).

We found that expression of gADF7-EGFP$_{V10}$ in *adf7* plants fully rescued the LatB-resistant germination and pollen tube elongation phenotypes (see Supplemental Figures 5C and 5D online), suggesting that ADF7-EGFP$_{V10}$ is fully functional and faithfully represents the subcellular localization of ADF7. ADF7-EGFP$_{V10}$ primarily decorated longitudinal actin cables in pollen

tubes of different lengths (Figures 4B to 4D), suggesting that ADF7 may regulate the dynamics of longitudinal actin cables. None of the other ADF7-EGFP fusion proteins formed obvious filamentous structures in pollen grains and tubes (see Supplemental Figure 5E online), suggesting that decoration of filamentous actin is vital for ADF7 function in vivo. Biochemical characterization of these ADF7-EGFP fusions and careful comparisons between them and the wild-type protein can provide significant insight into the mechanism of action of ADF7. In addition to ADF7-EGFP$_{V10}$, ADF7-EGFP$_{D75}$ was also selected for biochemical analysis because this fusion was comparable to the previously characterized yeast cofilin fusion (Okreglak and Drubin, 2007). Both ADF7-EGFP$_{V10}$ and ADF7-EGFP$_{D75}$ retain reasonable levels of G-actin binding activity (see Supplemental Figure 7D online), consistent with homology modeling results showing that the location of the GFP fusion is quite distal to the G-actin binding surface of ADF/cofilin and is therefore unlikely to affect G-actin binding (see Supplemental Figure 8A online). This could be the reason that the authors initially selected that location to insert GFP (Okreglak and Drubin, 2007). By contrast, we showed that none of the other constructs generated using a similar internal fusion strategy were functional in vivo (see Supplemental Figures 5C and 5D online). Compared with ADF7-EGFP$_{V10}$, ADF7-EGFP$_{D75}$ bound to F-actin poorly and could not sever actin filaments (see Supplemental Figures 7B to 7D online), potentially due to proximity to the adjacent actin monomer at D75 compared with V10 (see Supplemental Figure 8B online). This proximity may generate increased steric hindrance, affecting binding of the protein to F-actin. Certainly, it is also possible that this GFP fusion results in a conformational change in ADF7 and yeast cofilin that differentially affects activity.

The localization pattern of ADF7 is different from that of tobacco (*Nicotiana tabacum*) ADF1 (Nt ADF1). GFP-Nt ADF1 (with GFP fused at its N terminus) is concentrated at the subapical region of pollen tubes (Chen et al., 2002), and similar localization was also observed by immunostaining using an ADF antibody in lily pollen tubes (Lovy-Wheeler et al., 2006). However, we found that ADF7-EGFP$_{V10}$ was primarily concentrated on longitudinal actin cables (Figure 4). Our localization pattern of ADF7-EGFP$_{V10}$ is slightly different from that reported by Bou Daher et al. (2011) with the same fusion construct. The resulting difference could be due to the presence of wild-type ADF7 protein that may somehow interfere with the localization of ADF7-EGFP$_{V10}$ in pollen grains or tubes, since the construct was transformed into wild-type plants (Bou Daher et al., 2011). Based on our results demonstrating that ADF7-EGFP with EGFP fused at its N terminus cannot rescue *adf7* phenotypes (see Supplemental Figures 5C and 5D online), previous localization data for N-terminal ADF fusions must be cautiously interpreted. The subcellular localization pattern of ADF7 is also different from that of LlADF1, which has been shown to decorate actin filaments in pollen grains, but to be cytoplasmic in pollen tubes (Allwood et al., 2002). ADF was found by immunostaining to concentrate at pollen tube tips in daffodil (*Narcissus pseudonarcissus*) (Smertenko et al., 2001), which differs from the localization of ADF7 (Figure 4; Bou Daher et al., 2011) and ADF10 (Bou Daher et al., 2011), as minimal localization to the apical regions of pollen tubes was observed for these proteins. Certainly, we cannot rule out the possibility that the localization pattern of ADFs in the pollen tube may vary between species.

ADF7 Is Less Potent Than ADF1 in Promoting Actin Turnover

Our study verified that ADF7 is a typical ADF but found that it is less potent than ADF1 (Figure 3E; see Supplemental Figure 4 online). Side-by-side comparison of the activities of ADF7 and ADF1 showed that ADF7 has lower severing and monomer binding activities than ADF1 (Figures 3B, 3C, and 3H; see Supplemental Table 1 online), providing a detailed molecular explanation underlying their observed difference in activity. Our study, along with a previous report on pollen ADF1 in daffodil (Smertenko et al., 2001), suggests that weak depolymerizing activity might be a common phenomenon for pollen ADFs and implies that the biochemical nature of pollen ADFs might be well suited for pollen-specific functions. On the other hand, this observation also implies that pollen ADFs may be structurally different from vegetative ADFs. In support of this idea, polyclonal antisera raised against vegetative Zm-ADF3 cannot cross-react with pollen ADFs (Jiang et al., 1997), and amino acid sequence identity has been shown to be higher among pollen ADFs from different species than among ADFs from different tissues in the same plant (Lopez et al., 1996).

In addition to ADFs, a difference in activity between pollen profilin and vegetative profilin has also been reported (Kovar et al., 2000a). Furthermore, *Arabidopsis* actins were demonstrated to be functionally nonequivalent, as ectopic expression of a pollen actin in vegetative tissues resulted in dramatic phenotypes (Gilliland et al., 2002; Kandasamy et al., 2002) that were partially suppressed by coexpression of either the pollen ADF or profilin (Kandasamy et al., 2007). These data suggest that actin and its associated proteins coevolve to fulfill specific functions in distinct cell types, tissues, and organs, supporting the isovariant dynamics model (Meagher et al., 1999). An increase in the number and functional diversity of plant ADFs would be expected to be a part of this model. Within this framework, ADF7 evolved to fulfill pollen-specific requirements for actin dynamics. ADF7 mainly decorates longitudinal actin cables (Figure 4; Bou Daher et al., 2011), which have been demonstrated to be relatively stable in pollen tubes (Gibbon et al., 1999; Vidali et al., 2001). Thus, we propose that the biochemical activity of ADF7 is well suited for regulation of actin cable dynamics. Profilin and ADF have been demonstrated to act synergistically to increase actin turnover in vitro (Blanchoin and Pollard, 1998; Didry et al., 1998; Chaudhry et al., 2007; Michelot et al., 2007). As profilin is a uniformly distributed cytosolic protein (Vidali and Hepler, 1997), the low monomer sequestering activity of pollen profilin (Kovar et al., 2000a) along with the low actin depolymerizing activity of pollen ADFs (Smertenko et al., 2001; this study) may at least partially explain the relative stability and long lifespan of longitudinal actin cables.

METHODS

Arabidopsis thaliana Growth Conditions and Complementation

Arabidopsis plants (Col-0) were grown in a culture room at 22°C under a 16-h-light/8-h-dark cycle. To complement the phenotypes associated

with *adf7* (Salk_024576), a 4.6-kb genomic DNA fragment harboring the *ADF7* coding sequence (CDS) was amplified from *Arabidopsis* wild-type Col-0 genomic DNA using the primer pair G01/G02 (see Supplemental Table 2 online). The sequence of the cloned fragment was confirmed by DNA sequencing, and the fragment was subcloned into pCAMBIA1301 vector cut with *Sma*I-*Sal*I to yield the complementation construct. The resulting construct was subsequently transformed into *adf7* to generate the transgenic plants designated as gADF7;*adf7*.

RT-PCR Analysis

To investigate *ADF7* transcript levels, open flowers with mature pollens were collected. Total RNA was extracted using Trizol reagent (Invitrogen), and cDNA was synthesized using M-MLV (Promega) according to the manufacturer's instructions. *ADF7* transcript levels were compared between wild-type, *adf7*, and gADF7;*adf7* plants by amplifying a fragment using the primer pair R03/R04 (see Supplemental Table 2 online). To determine the levels of *ADF7* transcripts in transgenic plants harboring different ADF7-EGFP fusion constructs, two rounds of RT-PCR were performed. Initially, the relative amounts of *ADF7* transcripts between the transgenic plants were assessed by amplifying *EGFP* using the primer pair E01/E02 (see Supplemental Table 2 online). Subsequently, *ADF7* transcripts were amplified from transgenic plants harboring N-terminal and C-terminal EGFP fusion constructs using primer pairs R03/R05 and R06/R04 (see Supplemental Table 2 online). These levels were compared with the relative amount of *ADF7* transcripts in wild-type plants amplified using the primer pair R03/R04 (see Supplemental Table 2 online). *eIF4A* was amplified using primer pair R01/R02 (see Supplemental Table 2 online) as the internal control for normalization. The bands on agarose gel were stained with ethidium bromide, photographed, and compared by densitometry using ImageJ software (http://rsbweb.nih.gov/ij/; version 1.38).

Pollen Germination and Observation of Pollen Tube Growth

Pollen grains were cultured at 28°C on solid pollen GM [0.01% (w/v) H_3BO_3, 1 mM $CaCl_2$,1 mM $Ca(NO_3)_2$,1 mM $MgSO_4$,18% (w/v) Suc, and 0.5% (w/v) agar, pH 7.0] as previously described (Wu et al., 2010; Zhang et al., 2010). To determine the pollen germination rate, pollen grains were germinated on solid GM for 150 min. Pollen grains were subsequently observed under an Olympus IX71 microscope equipped with a ×10 objective, and images were acquired using a Retiga EXi Fast 1394 charge-coupled device (CCD) camera with Image-Pro Express 6.3 software. More than 500 pollen grains were counted for germination rate analysis per experiment, and each experiment was repeated five times for each genotype. To determine the effect of LatB on pollen germination, various concentrations of LatB were included in the solid GM. To determine the pollen tube growth rate, images of elongating pollen tubes were captured after germination for 60 and 90 min on GM. The average lengths of the pollen tubes at 60 min was subtracted from that at 90 min to obtain the average increase in length, which was then divided by the time interval to yield the average tube growth rate. More than 30 pollen tubes were chosen for tube elongation rate analysis for each experiment, and five and three independent experiments were performed for each genotype in the absence and presence of LatB, respectively.

Plasmid Construction for Analyzing the Subcellular Localization of ADF7

Several GFP fusion constructs were generated to assess the subcellular localization of ADF7. Initially, a 1.8-kb genomic DNA fragment containing the promoter, 5′-untranslated region, and coding region of *ADF7* was amplified using the primer pair G03/G04 (see Supplemental Table 2 online) as described by Bou Daher et al. (2011). This fragment was subsequently used as the template to amplify two consecutive upstream and downstream fragments, allowing for the fusion of EGFP (amplified with primer pair E01/E02; see Supplemental Table 2 online) between them. The construct with EGFP fused after Val10 (V10) of ADF7 (designated as gADF7-$EGFP_{V10}$) was made exactly as described by Bou Daher et al. (2011). Selection of the location of the EGFP insertion for several other ADF7 intramolecular fusion constructs was performed based on studies by Okreglak and Drubin (2007). Briefly, the structure of ADF7 was first generated using the structure of yeast cofilin as the template (PDB code 1CFY). We performed a structural alignment with yeast cofilin in order to select amino acids of ADF7 corresponding to the previously described GFP fusion with yeast cofilin (Okreglak and Drubin, 2007). The selected amino acids were Ile-73, Thr-74, Asp-75, Glu-76, Asn-77, and Cys-78 in ADF7. The primers used to generate the constructs are shown in Supplemental Table 2 online.

Actin Staining in Pollen Grains and Pollen Tubes

Actin filaments in pollen grains and tubes were stained with Alexa-488 phalloidin as previously described (Ye et al., 2009; Wu et al., 2010; Zhang et al., 2010). To determine the effect of LatB on the actin cytoskeleton, pollen grains were treated with 200 nM LatB for 30 min, and the actin cytoskeleton was visualized by staining with Alexa-488 phalloidin. To observe the actin cytoskeleton in pollen tubes, pollen grains were germinated for 75 min at 28°C on solid GM and were subsequently subjected to fixation and staining with Alexa-488 phalloidin. Actin filaments were observed with a confocal laser scanning microscope (Leica TCS SP5) equipped with a ×100 oil objective (1.46–numerical aperture HC PLAN). The fluorescent phalloidin was excited with the 488-nm line of an argon laser, and optical sections were collected with a step size of 0.5 μm for both pollen grains and tubes. The images shown are projections from all optical sections. The architecture of actin cytoskeleton was analyzed within different regions of pollen tubes. The regions 0 to 3 μm, 3 to 10 μm, and more than 10 μm away from the tip were defined as apex, subapex, and shank, respectively. The relative amount of actin filaments in pollen grains or tubes was quantified by measuring the fluorescence pixel intensity using ImageJ software (http://rsbweb.nih.gov/ij/; version 1.38). Skewness of actin filament staining was analyzed as described by Higaki et al. (2010). The width of filamentous structures was determined roughly according to the method described by Wu et al. (2010). For a particular filamentous structure, three vertical lines were drawn across it to obtain three values of width of fluorescence pixel intensity at the half height, and the final value of width for the particular filament was yielded by averaging them. To avoid repetitive counting, three or four optical sections were excluded between sections used for analysis in each pollen tube.

Live-Cell Imaging and Quantification of Actin Filaments in Pollen Tubes

Actin filaments were labeled with EGFP-lifeact expressed under control of the Lat52 promoter in pollen tubes as previously described by Vidali et al. (2009). Pollen grains were cultured at 28°C on solid pollen GM for 2 h until the average length of the pollen tubes was ~200 μm and were observed under an Olympus BX61 inverted microscope equipped with a ×100 Universal Plan Super Apochromat Objective (numerical aperture of 1.4) objective. Actin filaments were imaged using a spinning disk confocal microscope equipped with a Yokogawa CSU-X1 spinning disk head. Images were collected with a 512 × 512 Andor iXON electron multiplying CCD camera every 2 s. GFP was excited with a 488-nm laser, and the emitted fluorescence was collected using a 525/50-nm band-pass filter.

To measure the dynamic parameters associated with single filaments turnover, we initially defined properties for them. We randomly hand-selected

more than 300 filamentous actin structures from 15 wild-type pollen tubes to measure their fluorescence pixel intensity and width. The fluorescence pixel intensity of each filamentous structure was determined by drawing a line along it using the "measure" tool in ImageJ, and the average fluorescence pixel intensity was calculated in Kaleidagraph (Synergy Software; version 4.03). The kernel density of fluorescence pixel intensity distribution was processed using R programming language (http://www.R-project.org; version 2.15.1) as previously described (Qu et al., 2013). The width of filamentous structures was determined as described above. The filamentous structures with smaller intensity values form a population and are assumed to be single filaments. The filamentous structures with intensity values fall within this population from wild-type and *adf7* pollen tubes were selected for further analysis. For analyzing the stochastic dynamic parameters related to single filament turnover, only filaments longer than 2 μm and existing for more than 10 s were selected. Severing frequency (defined as the number of breaks per unit length per unit time; breaks/μm/s), maximum filament length, maximum filament lifetime. and elongation and depolymerization rate were determined and calculated roughly as previously described (Staiger et al., 2009; Henty et al., 2011). Briefly, the severing frequency was determined by counting all severing events from the filament reaching its maximum length to its disappearance. If a filament regrew after breaking, the length before breaking was taken as its maximum length and the time before breaking was taken as the valid time. The longest length of a tracked filament during its growth and shrinking was taken as the maximum filament length. Maximum filament life time was defined as the elapsed time for a filament from its appearance to its disappearance. Filament elongation and depolymerization rates were calculated as the changes of length versus the time intervals (Δlength/Δtime) in Excel. Only filaments continuously growing or shrinking for at least 10 s were taken into account.

To analyze the bundling and debundling frequency in shanks of pollen tubes, we selected a 10 × 6-μm^2 region that was 20 μm away from the tip to perform the analysis. The dynamics of actin bundles in this region was tracked in a consecutive 60 s and analyzed. The bundling and debundling frequencies were defined as the number of these events per unit area per unit time (events/μm^2/s).

Protein Production

Total RNA was isolated from flowers of wild-type, gADF7-$EGFP_{V10}$:*adf7*, and gADF7-$EGFP_{D75}$;*adf7* plants using Trizol reagent, and the corresponding cDNA was subsequently synthesized using M-MLV according to the manufacturer's instructions. Since the CDSs of *ADF7* and *ADF10* share 91.6% nucleotide identity, one primer pair R03/R04 (see Supplemental Table 2 online) derived from the *ADF7* untranslated region was used to specifically amplify *ADF7* cDNA using wild-type cDNA as the template. The resulting product was subsequently used as the template to amplify the CDS of *ADF7* using the primer pair P01/P02 (see Supplemental Table 2 online). After verification of the correct sequence by DNA sequencing analysis, the *ADF7* CDS was subcloned into the pGEX-KG vector to generate the pGEX-KG-ADF7 construct. Similarly, the CDSs for ADF7-$EGFP_{V10}$ and ADF7-$EGFP_{D75}$ were amplified using primer pair P01/P02 (see Supplemental Table 2 online) and cDNA derived from gADF7-$EGFP_{V10}$:*adf7* and gADF7-$EGFP_{D75}$;*adf7* as templates. The resulting products were verified by sequencing and subcloned into pGEX-KG cut with *Eco*RI-*Nco*I to produce the pGEX-KG-ADF7-$EGFP_{V10}$ and pGEX-KG-ADF7-$EGFP_{D75}$ constructs. The ADF7-$EGFP_{V10}$ CDS and the ADF7-$EGFP_{D75}$ CDS were also amplified with primer pair P03/P04 (see Supplemental Table 2 online), verified by DNA sequencing, and subcloned into the pET28a vector cut with *Nde*I-*Hin*dIII to generate the pET28a-ADF7-$EGFP_{V10}$ and pET28a-ADF7-$EGFP_{D75}$ constructs. Because EGFP interferes with the NBD-actin binding assay due to overlap of the wavelengths associated with absorption and emission of EGFP and NBD, we eliminated this effect by deleting three key amino acids (65T/66Y/67G) within the fluorophore center of EGFP. Thus, the plasmids, pET28a-ADF7-$EGFP_{V10}$ and pET28a-ADF7-$EGFP_{D75}$, were used as templates to generate the mutant constructs, pET28a-ADF7-mu$EGFP_{V10}$ and pET28a-ADF7-mu$EGFP_{D75}$, respectively, using primer pair P05/P06 (see Supplemental Table 2 online). To generate recombinant proteins, these expression constructs were transformed into the *Escherichia coli* BL21 (DE3) strain. Expression of these recombinant proteins was induced by the addition of 0.4 mM isopropyl β-D-thiogalactopyranoside, followed by incubation at 37°C for 4 h. Cells were harvested by centrifugation at 4000*g* for 10 min and lysed by sonication. GST fusion proteins were purified using glutathione-sepharose resin according to the manufacturer's recommended protocol. To produce ADF7 lacking a tag, GST-ADF7 was digested with thrombin (Sigma-Aldrich) overnight at 4°C to cleave GST. ADF7 was further purified by Q-sepharose chromatography (Amersham Biosciences). After loading onto a Q-sepharose column, ADF7 was eluted with elution buffer (10 mM Tris-HCl, pH 8.0, 100 mM KCl, and 1 mM DTT) after extensive washing with wash buffer (10 mM Tris-HCl, pH 8.0, and 1 mM DTT). The 6His-ADF7-$EGFP_{V10}$, 6His-ADF7-$EGFP_{D75}$, 6His-ADF7-mu$EGFP_{V10}$, and 6His-ADF7-mu$EGFP_{D75}$ fusion proteins were purified with nickel-nitriloacetic acid resin (Novagen) according to the manufacturer's instructions. All purified proteins were dialyzed against 5 mM Tris-HCl, pH 8.0, flash frozen in liquid nitrogen, and stored at −80°C. ADF1 was purified as described by Carlier et al. (1997). Actin was purified from rabbit skeletal muscle acetone powder as previously described (Spudich and Watt, 1971), and monomeric Ca^{2+}-ATP-actin was purified using Sephacryl S-300 chromatography in buffer G (5 mM Tris-HCl, pH 8.0, 0.2 mM ATP, 0.1 mM $CaCl_2$, 0.5 mM DTT, and 0.1 mM NaN_3) at 4°C (Pollard, 1984).

F-Actin High-Speed Cosedimentation Assay

A high speed cosedimentation assay was adapted from previously published methods (Kovar et al., 2000b; Huang et al., 2005). All proteins, including G-actin, were preclarified at 160,000*g* for 30 min at 4°C. Actin filaments (3 μM) were incubated with increasing concentrations (1 to 30 μM) of ADF7 or ADF1 or a constant concentration (5 and 10 μM) of GST-ADF7-$EGFP_{V10}$ or GST-ADF7-$EGFP_{D75}$. After incubation for 30 min at 25°C, the reaction mixtures were centrifuged at 100,000*g* for 30 min at 4°C. Fractions containing the supernatants and pellets were resolved by SDS-PAGE, and the gels were stained with Coomassie Brilliant Blue R 250 (Sigma-Aldrich). The amount of actin in the supernatant or pellet was quantified by densitometry using ImageJ (http://rsbweb.nih.gov/ij/; version 1.38).

Fluorescence Microscopy of Actin Filaments

Actin (4 μM) was incubated at 25°C for 30 min in polymerization buffer (10 mM imidazole, pH 7.0, 2 mM $MgCl_2$, 0.2 mM ATP, 50 mM KCl, 1 mM EGTA, 0.2 mM $CaCl_2$, 0.5 mM DTT, and 3 mM NaN_3). The resulting actin filaments (4 μM) were then incubated with varying concentrations of ADF7 or ADF1 for 3 min. An equimolar amount of Rhodamine-phalloidin (Sigma-Aldrich) was then added to label actin filaments and stop the reaction as described by Shi et al. (2013). Finally, actin filaments were diluted to 10 nM with fluorescence buffer (10 mM imidazole-HCl, pH 7.0, 50 mM KCl, 1 mM $MgCl_2$, 100 mM DTT, 100 μg/mL Glc oxidase, 15 μg/mL Glc, 20 μg/mL catalase, and 0.5% methylcellulose). A sample of 2.5 μL of the actin filament mixture was then placed on a 22 × 22-mm cover slip coated with 0.01% poly-L-Lys. Actin filaments were visualized by epifluorescence illumination under an Olympus IX71 microscope equipped with a ×60 oil objective (1.42 numerical aperture). Images were captured using a Retiga EXi Fast 1394 CCD camera (QImaging) with Image-Pro Express 6.3 software. The length of individual

actin filaments was quantified using ImageJ (http://rsbweb.nih.gov/ij/; version 1.38).

Light Scattering

All proteins and buffers were clarified by centrifugation at 200,000*g* for 60 min at 4°C prior to the assay. Actin (5 μM) was polymerized at 25°C for 2 h in polymerization buffer (described above). The resulting actin filaments (0.5 μM) were then incubated with varying concentrations of ADF7 or ADF1 in 1× KMEI (10 mM imidazole-HCl, pH 7.0, 50 mM KCl, 1 mM $MgCl_2$, and 1 mM EGTA). The absorbance associated with light scattering was monitored for 30 min using a QuantaMaster Luminescence QM 3 PH fluorometer (Photon Technology International) with both emission and excitation wavelengths set at 450 nm.

Direct Visualization of Actin Filament Severing and Depolymerization by TIRF Microscopy

Actin was labeled with 5-(and-6)-carboxytetramethylrhodamine-succinimidyl-ester, and the flow cell was prepared as previously described (Amann and Pollard, 2001). The flow cell was incubated with 25 nM N-ethylmaleimide-myosin for 2 min, followed by washing with 1% BSA for 3 min. It was next injected with 1× TIRF microscopy buffer (10 mM imidazole, pH 7.0, 50 mM KCl, 1 mM $MgCl_2$, 1 mM EGTA, 50 mM DTT, 0.2 mM ATP, 50 μM $CaCl_2$, 15 mM Glc, 20 μg/mL catalase, 100 μg/mL Glc oxidase, and 0.5% methylcellulose). Actin filaments (100 nM; 50% rhodamine-labeled) were injected into the chamber, and the mixture was incubated for 3 min in the dark. Finally, the flow cell was washed with 1× TIRF microscopy buffer to remove free actin filaments that were not attached to NEM-myosin. Single actin filaments were observed by TIRF illumination with an Olympus IX81 microscope equipped with a ×100 oil objective (1.49 numerical aperture). Images were collected for 5 min with an interval of 3 or 1 s using a Photometrics cascade II 512 CCD camera (Major Instruments) with microManager software. To determine the filament severing activity of ADF7, ADF1, 6His-ADF7-$EGFP_{V10}$, and 6His-ADF7-$EGFP_{D75}$, varying concentrations of these proteins were injected into the chamber in 1× TIRF microscopy buffer. The filament severing frequency was defined as breaks/μm/s as previously reported (Andrianantoandro and Pollard, 2006). More than 20 actin filaments with lengths >10 μm were selected for quantification of actin filament severing frequency. The monomer dissociation rate (subunits/s) was determined assuming 1-μm-length filament equals 334 subunits. The definition for the pointed end and barbed end of each measured filament in the absence or presence of ADF proteins was according to the description by Shi et al. (2013).

Binding of ADF to G-Actin

G-actin binding activity of ADF7 or ADF1 was determined by measuring the decrease in fluorescence of NBD-labeled actin. NBD-G-actin was prepared as previously described (Detmers et al., 1981). NBD-ATP-actin or NBD-ADP-actin was prepared as described by Chaudhry et al. (2007). For the preparation of NBD-ATP-G-actin, 20 μM NBD-actin was incubated with 1 mM ATP for 70 min at 4°C in the dark. For the preparation of NBD-ADP-G-actin, 20 μM NBD-actin was incubated with 20 units/mL of hexokinase (Sigma-Aldrich) and 1 mM Glc for 3 h at 4°C in the dark. NBD-ATP-G-actin or NBD-ADP-G-actin (0.2 μM) was then incubated with increasing concentrations of ADF7, ADF1, 6His-ADF7-muEGFP$_{D75}$, or 6His-ADF7-muEGFP$_{V10}$ in 1 mM $MgCl_2$ and 100 mM KCl. The change in NBD fluorescence was analyzed for 20 s using a QuantaMaster Luminescence QM 3 PH fluorometer with the excitation and emission wavelengths set to 475 and 530 nm, respectively. The resulting data were fitted using Kaleidagraph (Synergy Software; version 3.6) with the following equations (Carlier et al., 1997):

$$Q = \frac{F_0 - F_{(+\mathrm{ADF})}}{F_0} \quad (1)$$

$$\frac{1}{\alpha} = 1 + \frac{\mathrm{Kd}}{[\mathrm{ADF}]} \quad (2)$$

$$[\mathrm{ADF}] = \frac{[\mathrm{ADF}]_0 - [\mathrm{G}]_0 - \mathrm{K_d} \pm \sqrt{([\mathrm{ADF}]_0 - [\mathrm{G}]_0 - \mathrm{K_d})^2 + 4\mathrm{K_d}[\mathrm{ADF}]_0}}{2} \quad (3)$$

where α = Q/Qmax, Q_{max} is the maximum fluorescence quenching caused by the saturation of G-actin bound to ADF, $[ADF]_0$ is the total concentration of ADF, $[G]_0$ is the total concentration of G-actin, and K_d is the equilibrium dissociation constant of the G-actin-ADF complex.

Nucleotide Exchange Analysis

The rate of G-actin nucleotide exchange was determined by measuring the increase in fluorescence upon binding of 1,N^6-ethenoadenosine 5′-triphosphate (ε-ATP; Sigma-Aldrich). The experiment was performed as described by Chaudhry et al. (2010). Briefly, 2 μM ADP-actin in buffer G lacking ATP was incubated with Tris/NaCl buffer (20 mM Tris-HCl, pH 8.0, and 50 mM NaCl) alone or containing ADF7 or ADF1. Next, 50 μM ε-ATP (Molecular Probes) was added to the solution. The reaction was monitored using a QuantaMaster Luminescence QM 3 PH fluorometer for a minimum of 10 min with the excitation and emission wavelengths set at 350 and 410 nm, respectively.

Determination of Actin Filament Turnover Rate

The actin filament turnover rate was quantified as previously described (Didry et al., 1998; Chaudhry et al., 2007). Fluorescently labeled ε-ADP-actin filaments were preassembled from ε-ATP-actin subunits, and the turnover rate was determined by measuring the change in fluorescence caused by exchange of ε-ADP for nonfluorescent ATP. εATP-G-actin was prepared as previously described (Valentin-Ranc and Carlier, 1989), and 15 μM εATP-G-actin was assembled in the presence of 30 μM εATP in 1× KMEI (50 mM KCl, 1 mM $MgCl_2$, 1 mM EGTA, and 10 mM imidazol-HCl, pH 7.0). Subsequently, 4 μM εADP-actin filaments were incubated with 5 μM ADF7 or 5 μM ADF1 for 20 min in 1× KMEI. The change in the fluorescence at 25°C was analyzed after the addition of 1 mM ATP using a QuantaMaster Luminescence QM 3 PH fluorometer. The excitation and emission wavelengths were 350 and 410 nm, respectively.

Sequence Alignment and Three-Dimensional Homology Modeling

Sequence alignment was performed using the online software program ClustalW (http://www.genome.jp/tools/clustalw/). The resulting data were saved as an .aln file and submitted to the online server ESPript2.2 (http://espript.ibcp.fr/ESPript/cgi-bin/ESPript.cgi) to predict the secondary structures and calculate the amino acid similarity based on the Risler matrix method with the global score set to 0.7. The crystal structure of yeast cofilin (PDB ID: 1COF) and a predicted three-dimensional structure of ADF7 that was generated by homology modeling using the crystal structure of ADF1 (PDB ID:1F7S) as a template were used to improve the alignment results. The structure of the ADF7 (pink)/Actin1 (green) complex was generated by SWISS-MODEL (http://swissmodel.expasy.org/SWISS-MODEL.html) using the known crystal structure of rabbit alpha skeletal muscle actin/mouse twinfilin1 C-terminal ADF-H domain (Twf-C)

complex as the template (PDB ID: 3DAW). The structure was displayed with PyMOL (version 1.4.1; DeLano Scientific). A simulation model of an actin filament decorated with ADF7 was generated based on the PDB ID 3J0S template, in which each human cofilin-2 was replaced with ADF7.

Accession Numbers

Sequence data from this article can be found in the Arabidopsis Genome Initiative and GenBank/UniProtKB under accession numbers At4g25590 (*ADF7*), AAA13256.1 (*Saccharomyces cerevisiae* cofilin), Q39250 (ADF1), Q91YR1 (*Mus musculus* Twifilin1), P68135 (*Oryctolagus cuniculus* alpha skeletal muscle actin), P0CJ46 (*Arabidopsis* Actin1), P60706 (*Gallus gallus* cytoplasmic actin1), and P23528 (*Homo sapiens* cofilin2).

Supplemental Data

The following materials are available in the online version of this article.

Supplemental Figure 1. Loss of *ADF7* Does Not Affect Pollen Germination.

Supplemental Figure 2. No Change in F-Actin Levels Was Detected in *adf7* Pollen Grains.

Supplemental Figure 3. Loss of *ADF7* Renders Pollen Germination Resistant to LatB.

Supplemental Figure 4. ADF7 Depolymerizes Actin Filaments but Is less Potent Than ADF1.

Supplemental Figure 5. ADF7-EGFP$_{V10}$ Is Fully Functional.

Supplemental Figure 6. The Distribution of Fluorescence Pixel Intensity and Width of Filamentous Structures in Wild-Type Pollen Tubes.

Supplemental Figure 7. ADF7-EGFP$_{V10}$ Retains Both G-Actin Binding and Filament Severing Activity, Whereas ADF7-EGFP$_{D75}$ Retains G-Actin Binding Activity but Is Deficient in Severing Actin Filaments.

Supplemental Figure 8. Homology Modeling of Three-Dimensional Structures of the ADF7/Actin Complex and ADF7-Decorated F-Actin.

Supplemental Table 1. The Binding Affinity of ADF Proteins to NBD-ADP-Actin and NBD-ATP-Actin.

Supplemental Table 2. Primers Sequences Used in This Study.

Supplemental Movie 1. Time-Series Movie of Actin Filament Severing in the Absence of ADF7.

Supplemental Movie 2. Time-Series Movie of Actin Filament Severing in the Presence of 200 nM ADF7.

Supplemental Movie 3. Time-Series Movie Displaying the Severing Events of Single Filaments in a Wild-Type Pollen Tube.

Supplemental Movie 4. Time-Series Movie Displaying the Severing Events of Single Filaments in an *adf7* Pollen Tube.

Supplemental Movie 5. Time-Series Movie Displaying the Depolymerization of a Single Filament in a Wild-Type Pollen Tube.

Supplemental Movie 6. Time-Series Movie Displaying the Depolymerization of a Single Filament in an *adf7* Pollen Tube.

Supplemental Movie 7. Time-Series Movie Displaying the Formation of a Thick Bundle in a Wild-Type Pollen Tube.

Supplemental Movie 8. Time-Series Movie Displaying the Debundling Event of a Thick Bundle in a Wild-Type Pollen Tube.

Supplemental Movie Legends 1. Brief Descriptions of Supplemental Movies 1-8.

ACKNOWLEDGMENTS

We thank the ABRC for providing the T-DNA insertion line and members of the Huang lab for stimulating discussions. We also thank Christopher J. Staiger (Purdue University) for the ADF1 expression clone. This work was supported by grants from the Ministry of Science and Technology of China (2013CB945100 and 2011CB944600) and the National Natural Science Foundation of China (31125004 and 31121065).

AUTHOR CONTRIBUTIONS

S.H. conceived the research. Y.Z., Y.X., Y.J., and S.H. designed the research. Y.Z., Y.X., Y.J., and X.Q. performed the experiments. Y.Z., Y.X., Y.J., X.Q., and S.H. analyzed the data. Y.Z., Y.X., Y.J., and S.H. wrote the article.

Received August 26, 2013; revised August 26, 2013; accepted September 2, 2013; published September 20, 2013.

REFERENCES

Allwood, E.G., Smertenko, A.P., and Hussey, P.J. (2001). Phosphorylation of plant actin-depolymerising factor by calmodulin-like domain protein kinase. FEBS Lett. **499:** 97–100.

Allwood, E.G., Anthony, R.G., Smertenko, A.P., Reichelt, S., Drobak, B.K., Doonan, J.H., Weeds, A.G., and Hussey, P.J. (2002). Regulation of the pollen-specific actin-depolymerizing factor LIADF1. Plant Cell **14:** 2915–2927.

Amann, K.J., and Pollard, T.D. (2001). The Arp2/3 complex nucleates actin filament branches from the sides of pre-existing filaments. Nat. Cell Biol. **3:** 306–310.

Andrianantoandro, E., and Pollard, T.D. (2006). Mechanism of actin filament turnover by severing and nucleation at different concentrations of ADF/cofilin. Mol. Cell **24:** 13–23.

Augustine, R.C., Vidali, L., Kleinman, K.P., and Bezanilla, M. (2008). Actin depolymerizing factor is essential for viability in plants, and its phosphoregulation is important for tip growth. Plant J. **54:** 863–875.

Bamburg, J.R., and Bernstein, B.W. (2008). ADF/cofilin. Curr. Biol. **18:** R273–R275.

Bamburg, J.R., Harris, H.E., and Weeds, A.G. (1980). Partial purification and characterization of an actin depolymerizing factor from brain. FEBS Lett. **121:** 178–182.

Bao, C., Wang, J., Zhang, R., Zhang, B., Zhang, H., Zhou, Y., and Huang, S. (2012). *Arabidopsis* VILLIN2 and VILLIN3 act redundantly in sclerenchyma development via bundling of actin filaments. Plant J. **71:** 962–975.

Bernstein, B.W., and Bamburg, J.R. (2010). ADF/cofilin: A functional node in cell biology. Trends Cell Biol. **20:** 187–195.

Berro, J., Sirotkin, V., and Pollard, T.D. (2010). Mathematical modeling of endocytic actin patch kinetics in fission yeast: Disassembly requires release of actin filament fragments. Mol. Biol. Cell **21:** 2905–2915.

Blanchoin, L., and Pollard, T.D. (1998). Interaction of actin monomers with *Acanthamoeba actophorin* (ADF/cofilin) and profilin. J. Biol. Chem. **273:** 25106–25111.

Bou Daher, F., van Oostende, C., and Geitmann, A. (2011). Spatial and temporal expression of actin depolymerizing factors ADF7 and ADF10 during male gametophyte development in *Arabidopsis thaliana*. Plant Cell Physiol. **52:** 1177–1192.

Burgos-Rivera, B., Ruzicka, D.R., Deal, R.B., McKinney, E.C., King-Reid, L., and Meagher, R.B. (2008). ACTIN DEPOLYMERIZING FACTOR9 controls development and gene expression in *Arabidopsis*. Plant Mol. Biol. **68:** 619–632.

Carlier, M.F., Laurent, V., Santolini, J., Melki, R., Didry, D., Xia, G.X., Hong, Y., Chua, N.H., and Pantaloni, D. (1997). Actin depolymerizing factor (ADF/cofilin) enhances the rate of filament turnover: Implication in actin-based motility. J. Cell Biol. **136:** 1307–1322.

Chan, C., Beltzner, C.C., and Pollard, T.D. (2009). Cofilin dissociates Arp2/3 complex and branches from actin filaments. Curr. Biol. **19:** 537–545.

Chaudhry, F., Guérin, C., von Witsch, M., Blanchoin, L., and Staiger, C.J. (2007). Identification of *Arabidopsis* cyclase-associated protein 1 as the first nucleotide exchange factor for plant actin. Mol. Biol. Cell **18:** 3002–3014.

Chaudhry, F., Little, K., Talarico, L., Quintero-Monzon, O., and Goode, B.L. (2010). A central role for the WH2 domain of Srv2/CAP in recharging actin monomers to drive actin turnover in vitro and in vivo. Cytoskeleton (Hoboken) **67:** 120–133.

Chen, C.Y., Wong, E.I., Vidali, L., Estavillo, A., Hepler, P.K., Wu, H.M., and Cheung, A.Y. (2002). The regulation of actin organization by actin-depolymerizing factor in elongating pollen tubes. Plant Cell **14:** 2175–2190.

Chen, H., Bernstein, B.W., Sneider, J.M., Boyle, J.A., Minamide, L.S., and Bamburg, J.R. (2004). In vitro activity differences between proteins of the ADF/cofilin family define two distinct subgroups. Biochemistry **43:** 7127–7142.

Chen, N., Qu, X., Wu, Y., and Huang, S. (2009). Regulation of actin dynamics in pollen tubes: Control of actin polymer level. J. Integr. Plant Biol. **51:** 740–750.

Chen, Q., and Pollard, T.D. (2011). Actin filament severing by cofilin is more important for assembly than constriction of the cytokinetic contractile ring. J. Cell Biol. **195:** 485–498.

Cheung, A.Y., and Wu, H.M. (2008). Structural and signaling networks for the polar cell growth machinery in pollen tubes. Annu. Rev. Plant Biol. **59:** 547–572.

Clément, M., Ketelaar, T., Rodiuc, N., Banora, M.Y., Smertenko, A., Engler, G., Abad, P., Hussey, P.J., and de Almeida Engler, J. (2009). Actin-depolymerizing factor2-mediated actin dynamics are essential for root-knot nematode infection of *Arabidopsis*. Plant Cell **21:** 2963–2979.

Cooper, J.A. (1987). Effects of cytochalasin and phalloidin on actin. J. Cell Biol. **105:** 1473–1478.

Coué, M., Brenner, S.L., Spector, I., and Korn, E.D. (1987). Inhibition of actin polymerization by latrunculin A. FEBS Lett. **213:** 316–318.

Daher, F.B., and Geitmann, A. (2012). Actin depolymerizing factors ADF7 and ADF10 play distinct roles during pollen development and pollen tube growth. Plant Signal. Behav. **7:** 879–881.

Detmers, P., Weber, A., Elzinga, M., and Stephens, R.E. (1981). 7-Chloro-4-nitrobenzeno-2-oxa-1,3-diazole actin as a probe for actin polymerization. J. Biol. Chem. **256:** 99–105.

Didry, D., Carlier, M.F., and Pantaloni, D. (1998). Synergy between actin depolymerizing factor/cofilin and profilin in increasing actin filament turnover. J. Biol. Chem. **273:** 25602–25611.

Dong, C.H., Xia, G.X., Hong, Y., Ramachandran, S., Kost, B., and Chua, N.H. (2001). ADF proteins are involved in the control of flowering and regulate F-actin organization, cell expansion, and organ growth in *Arabidopsis*. Plant Cell **13:** 1333–1346.

Feng, Y., Liu, Q., and Xue, Q. (2006). Comparative study of rice and *Arabidopsis* actin-depolymerizing factors gene families. J. Plant Physiol. **163:** 69–79.

Geitmann, A., Snowman, B.N., Emons, A.M., and Franklin-Tong, V.E. (2000). Alterations in the actin cytoskeleton of pollen tubes are induced by the self-incompatibility reaction in *Papaver rhoeas*. Plant Cell **12:** 1239–1251.

Gibbon, B.C., Kovar, D.R., and Staiger, C.J. (1999). Latrunculin B has different effects on pollen germination and tube growth. Plant Cell **11:** 2349–2363.

Gilliland, L.U., Kandasamy, M.K., Pawloski, L.C., and Meagher, R.B. (2002). Both vegetative and reproductive actin isovariants complement the stunted root hair phenotype of the Arabidopsis act2-1 mutation. Plant Physiol. **130:** 2199–2209.

Gilliland, L.U., Pawloski, L.C., Kandasamy, M.K., and Meagher, R.B. (2003). *Arabidopsis* actin gene ACT7 plays an essential role in germination and root growth. Plant J. **33:** 319–328.

Giuliano, K.A., Khatib, F.A., Hayden, S.M., Daoud, E.W., Adams, M.E., Amorese, D.A., Bernstein, B.W., and Bamburg, J.R. (1988). Properties of purified actin depolymerizing factor from chick brain. Biochemistry **27:** 8931–8938.

Henty, J.L., Bledsoe, S.W., Khurana, P., Meagher, R.B., Day, B., Blanchoin, L., and Staiger, C.J. (2011). *Arabidopsis* actin depolymerizing factor4 modulates the stochastic dynamic behavior of actin filaments in the cortical array of epidermal cells. Plant Cell **23:** 3711–3726.

Hepler, P.K., Vidali, L., and Cheung, A.Y. (2001). Polarized cell growth in higher plants. Annu. Rev. Cell Dev. Biol. **17:** 159–187.

Higaki, T., Kutsuna, N., Sano, T., Kondo, N., and Hasezawa, S. (2010). Quantification and cluster analysis of actin cytoskeletal structures in plant cells: Role of actin bundling in stomatal movement during diurnal cycles in *Arabidopsis* guard cells. Plant J. **61:** 156–165.

Honys, D., and Twell, D. (2003). Comparative analysis of the Arabidopsis pollen transcriptome. Plant Physiol. **132:** 640–652.

Huang, S., Gao, L., Blanchoin, L., and Staiger, C.J. (2006). Heterodimeric capping protein from *Arabidopsis* is regulated by phosphatidic acid. Mol. Biol. Cell **17:** 1946–1958.

Huang, S., Robinson, R.C., Gao, L.Y., Matsumoto, T., Brunet, A., Blanchoin, L., and Staiger, C.J. (2005). *Arabidopsis* VILLIN1 generates actin filament cables that are resistant to depolymerization. Plant Cell **17:** 486–501.

Jiang, C.J., Weeds, A.G., and Hussey, P.J. (1997). The maize actin-depolymerizing factor, ZmADF3, redistributes to the growing tip of elongating root hairs and can be induced to translocate into the nucleus with actin. Plant J. **12:** 1035–1043.

Kandasamy, M.K., Burgos-Rivera, B., McKinney, E.C., Ruzicka, D.R., and Meagher, R.B. (2007). Class-specific interaction of profilin and ADF isovariants with actin in the regulation of plant development. Plant Cell **19:** 3111–3126.

Kandasamy, M.K., McKinney, E.C., and Meagher, R.B. (2002). Functional nonequivalency of actin isovariants in *Arabidopsis*. Mol. Biol. Cell **13:** 251–261.

Kost, B., Spielhofer, P., and Chua, N.H. (1998). A GFP-mouse talin fusion protein labels plant actin filaments in vivo and visualizes the actin cytoskeleton in growing pollen tubes. Plant J. **16:** 393–401.

Kovar, D.R., Drøbak, B.K., and Staiger, C.J. (2000a). Maize profilin isoforms are functionally distinct. Plant Cell **12:** 583–598.

Kovar, D.R., Staiger, C.J., Weaver, E.A., and McCurdy, D.W. (2000b). AtFim1 is an actin filament crosslinking protein from *Arabidopsis thaliana*. Plant J. **24:** 625–636.

Kueh, H.Y., Brieher, W.M., and Mitchison, T.J. (2010). Quantitative analysis of actin turnover in Listeria comet tails: Evidence for catastrophic filament turnover. Biophys. J. **99:** 2153–2162.

Li, X.B., Xu, D., Wang, X.L., Huang, G.Q., Luo, J., Li, D.D., Zhang, Z.T., and Xu, W.L. (2010). Three cotton genes preferentially expressed in flower tissues encode actin-depolymerizing factors which are involved in F-actin dynamics in cells. J. Exp. Bot. **61:** 41–53.

Lin, Y., and Yang, Z. (1997). Inhibition of pollen tube elongation by microinjected anti-Rop1Ps antibodies suggests a crucial role for Rho-type GTPases in the control of tip growth. Plant Cell **9:** 1647–1659.

Lopez, I., Anthony, R.G., Maciver, S.K., Jiang, C.J., Khan, S., Weeds, A.G., and Hussey, P.J. (1996). Pollen specific expression of maize genes encoding actin depolymerizing factor-like proteins. Proc. Natl. Acad. Sci. USA **93:** 7415–7420.

Lovy-Wheeler, A., Kunkel, J.G., Allwood, E.G., Hussey, P.J., and Hepler, P.K. (2006). Oscillatory increases in alkalinity anticipate growth and may regulate actin dynamics in pollen tubes of lily. Plant Cell **18:** 2182–2193.

Maciver, S.K., and Hussey, P.J. (2002). The ADF/cofilin family: Actin-remodeling proteins. Genome Biol. **3:** reviews3007.

Meagher, R.B., McKinney, E.C., and Kandasamy, M.K. (1999). Isovariant dynamics expand and buffer the responses of complex systems: The diverse plant actin gene family. Plant Cell **11:** 995–1006.

Michelot, A., Berro, J., Guérin, C., Boujemaa-Paterski, R., Staiger, C.J., Martiel, J.L., and Blanchoin, L. (2007). Actin-filament stochastic dynamics mediated by ADF/cofilin. Curr. Biol. **17:** 825–833.

Miller, D.D., de Ruijter, N.C.A., Bisseling, T., and Emons, A.M.C. (1999). The role of actin in root hair morphogenesis: Studies with lipochito-oligosaccharide as a growth stimulator and cytochalasin as an actin perturbing drug. Plant J. **17:** 141–154.

Okreglak, V., and Drubin, D.G. (2007). Cofilin recruitment and function during actin-mediated endocytosis dictated by actin nucleotide state. J. Cell Biol. **178:** 1251–1264.

Papuga, J., Hoffmann, C., Dieterle, M., Moes, D., Moreau, F., Tholl, S., Steinmetz, A., and Thomas, C. (2010). *Arabidopsis* LIM proteins: A family of actin bundlers with distinct expression patterns and modes of regulation. Plant Cell **22:** 3034–3052.

Pina, C., Pinto, F., Feijó, J.A., and Becker, J.D. (2005). Gene family analysis of the Arabidopsis pollen transcriptome reveals biological implications for cell growth, division control, and gene expression regulation. Plant Physiol. **138:** 744–756.

Pollard, T.D. (1984). Polymerization of ADP-actin. J. Cell Biol. **99:** 769–777.

Pollard, T.D., and Cooper, J.A. (2009). Actin, a central player in cell shape and movement. Science **326:** 1208–1212.

Qu, X., Zhang, H., Xie, Y., Wang, J., Chen, N., and Huang, S. (2013). *Arabidopsis* villins promote actin turnover at pollen tube tips and facilitate the construction of actin collars. Plant Cell **25:** 1803–1817.

Roland, J., Berro, J., Michelot, A., Blanchoin, L., and Martiel, J.L. (2008). Stochastic severing of actin filaments by actin depolymerizing factor/cofilin controls the emergence of a steady dynamical regime. Biophys. J. **94:** 2082–2094.

Ruzicka, D.R., Kandasamy, M.K., McKinney, E.C., Burgos-Rivera, B., and Meagher, R.B. (2007). The ancient subclasses of *Arabidopsis* Actin Depolymerizing Factor genes exhibit novel and differential expression. Plant J. **52:** 460–472.

Shi, M., Xie, Y., Zheng, Y., Wang, J., Su, Y., Yang, Q., and Huang, S. (2013). *Oryza sativa* actin-interacting protein 1 is required for rice growth by promoting actin turnover. Plant J. **73:** 747–760.

Skau, C.T., and Kovar, D.R. (2010). Fimbrin and tropomyosin competition regulates endocytosis and cytokinesis kinetics in fission yeast. Curr. Biol. **20:** 1415–1422.

Smertenko, A.P., Allwood, E.G., Khan, S., Jiang, C.J., Maciver, S.K., Weeds, A.G., and Hussey, P.J. (2001). Interaction of pollen-specific actin-depolymerizing factor with actin. Plant J. **25:** 203–212.

Snowman, B.N., Kovar, D.R., Shevchenko, G., Franklin-Tong, V.E., and Staiger, C.J. (2002). Signal-mediated depolymerization of actin in pollen during the self-incompatibility response. Plant Cell **14:** 2613–2626.

Spudich, J.A., and Watt, S. (1971). The regulation of rabbit skeletal muscle contraction. I. Biochemical studies of the interaction of the tropomyosin-troponin complex with actin and the proteolytic fragments of myosin. J. Biol. Chem. **246:** 4866–4871.

Staiger, C.J. (2000). Signaling to the actin cytoskeleton in plants. Annu. Rev. Plant Physiol. Plant Mol. Biol. **51:** 257–288.

Staiger, C.J., Poulter, N.S., Henty, J.L., Franklin-Tong, V.E., and Blanchoin, L. (2010). Regulation of actin dynamics by actin-binding proteins in pollen. J. Exp. Bot. **61:** 1969–1986.

Staiger, C.J., Sheahan, M.B., Khurana, P., Wang, X., McCurdy, D.W., and Blanchoin, L. (2009). Actin filament dynamics are dominated by rapid growth and severing activity in the *Arabidopsis* cortical array. J. Cell Biol. **184:** 269–280.

Su, H., Zhu, J., Cai, C., Pei, W., Wang, J., Dong, H., and Ren, H. (2012). FIMBRIN1 is involved in lily pollen tube growth by stabilizing the actin fringe. Plant Cell **24:** 4539–4554.

Suarez, C., Roland, J., Boujemaa-Paterski, R., Kang, H., McCullough, B.R., Reymann, A.C., Guérin, C., Martiel, J.L., De la Cruz, E.M., and Blanchoin, L. (2011). Cofilin tunes the nucleotide state of actin filaments and severs at bare and decorated segment boundaries. Curr. Biol. **21:** 862–868.

Taylor, L.P., and Hepler, P.K. (1997). Pollen germination and tube growth. Annu. Rev. Plant Physiol. Plant Mol. Biol. **48:** 461–491.

Tholl, S., Moreau, F., Hoffmann, C., Arumugam, K., Dieterle, M., Moes, D., Neumann, K., Steinmetz, A., and Thomas, C. (2011). *Arabidopsis* actin-depolymerizing factors (ADFs) 1 and 9 display antagonist activities. FEBS Lett. **585:** 1821–1827.

Thomas, C. (2012). Bundling actin filaments from membranes: Some novel players. Front. Plant Sci. **3:** 188.

Thomas, C., Tholl, S., Moes, D., Dieterle, M., Papuga, J., Moreau, F., and Steinmetz, A. (2009). Actin bundling in plants. Cell Motil. Cytoskeleton **66:** 940–957.

Tian, M., Chaudhry, F., Ruzicka, D.R., Meagher, R.B., Staiger, C.J., and Day, B. (2009). Arabidopsis actin-depolymerizing factor AtADF4 mediates defense signal transduction triggered by the *Pseudomonas syringae* effector AvrPphB. Plant Physiol. **150:** 815–824.

Valentin-Ranc, C., and Carlier, M.F. (1989). Evidence for the direct interaction between tightly bound divalent metal ion and ATP on actin. Binding of the lambda isomers of beta gamma-bidentate CrATP to actin. J. Biol. Chem. **264:** 20871–20880.

van der Honing, H.S., Kieft, H., Emons, A.M.C., and Ketelaar, T. (2012). Arabidopsis VILLIN2 and VILLIN3 are required for the generation of thick actin filament bundles and for directional organ growth. Plant Physiol. **158:** 1426–1438.

Vartiainen, M.K., Mustonen, T., Mattila, P.K., Ojala, P.J., Thesleff, I., Partanen, J., and Lappalainen, P. (2002). The three mouse actin-depolymerizing factor/cofilins evolved to fulfill cell-type-specific requirements for actin dynamics. Mol. Biol. Cell **13:** 183–194.

Vidali, L., and Hepler, P.K. (1997). Characterization and localization of profilin in pollen grains and tubes of *Lilium longiflorum*. Cell Motil. Cytoskeleton **36:** 323–338.

Vidali, L., and Hepler, P.K. (2001). Actin and pollen tube growth. Protoplasma **215:** 64–76.

Vidali, L., McKenna, S.T., and Hepler, P.K. (2001). Actin polymerization is essential for pollen tube growth. Mol. Biol. Cell **12:** 2534–2545.

Vidali, L., Rounds, C.M., Hepler, P.K., and Bezanilla, M. (2009). Lifeact-mEGFP reveals a dynamic apical F-actin network in tip growing plant cells. PLoS ONE **4:** e5744.

Wang, H.J., Wan, A.R., and Jauh, G.Y. (2008). An actin-binding protein, LILIM1, mediates calcium and hydrogen regulation of actin dynamics in pollen tubes. Plant Physiol. **147:** 1619–1636.

Wu, Y., Yan, J., Zhang, R., Qu, X., Ren, S., Chen, N., and Huang, S. (2010). *Arabidopsis* FIMBRIN5, an actin bundling factor, is required for pollen germination and pollen tube growth. Plant Cell **22:** 3745–3763.

Ye, J., Zheng, Y., Yan, A., Chen, N., Wang, Z., Huang, S., and Yang, Z. (2009). *Arabidopsis* formin3 directs the formation of actin cables and polarized growth in pollen tubes. Plant Cell **21:** 3868–3884.

Zhang, H., Qu, X., Bao, C., Khurana, P., Wang, Q., Xie, Y., Zheng, Y., Chen, N., Blanchoin, L., Staiger, C.J., and Huang, S. (2010). *Arabidopsis* VILLIN5, an actin filament bundling and severing protein, is necessary for normal pollen tube growth. Plant Cell **22:** 2749–2767.

Zhu, L., Zhang, Y., Kang, E., Xu, Q., Wang, M., Rui, Y., Liu, B., Yuan, M., and Fu, Y. (2013). MAP18 regulates the direction of pollen tube growth in *Arabidopsis* by modulating F-actin organization. Plant Cell **25:** 851–867.